



# Numerical model reduction with error control in computational homogenization of transient heat flow

Emil Aggestam\*, Fredrik Larsson, Kenneth Runesson, Fredrik Ekre

*Department of Applied Mechanics, Chalmers University of Technology, Gothenburg, S-41296, Sweden*

Received 18 November 2016; received in revised form 3 July 2017; accepted 8 August 2017

Available online 14 August 2017

---

## Abstract

Numerical Model Reduction (NMR) is exploited for solving the finite element problem on a Representative Volume Element (RVE) that arises from the computational homogenization of a model problem of transient heat flow. Since the problem is linear, an orthogonal basis is obtained via the classical method of spectral decomposition. A symmetrized version of the space–time variational format is adopted for estimating the error from the model reduction in (i) energy norm and in (ii) given Quantities of Interest. This technique, which was recently developed in the context of the (non-selfadjoint) stationary diffusion–convection problem, is novel in the present context of NMR. By considering the discrete, unreduced, model as exact, we are able to obtain guaranteed bounds on the error while using only the reduced basis and with minor computational effort. The performance of the error estimates is demonstrated via numerical results, where the subscale is modeled in both one and three spatial dimensions.

© 2017 The Authors. Published by Elsevier B.V. This is an open access article under the CC BY license (<http://creativecommons.org/licenses/by/4.0/>).

*Keywords:* Model reduction; Error control; Computational homogenization; Transient

---

## 1. Introduction

Computational homogenization is a well-established approach in material modeling with the purpose to account for strong micro-heterogeneity in an approximate, yet “sufficiently accurate”, fashion while reducing the computational cost as compared to Direct Numerical Simulation (DNS) of the fine-scale problem. When the intrinsic material properties are nonlinear and/or the subscale problem is inherently transient, it is necessary to resort to nested macro-subscale computations (Finite Element squared, FE<sup>2</sup>), whereby the subscale computations are carried out on a so called Representative Volume Element (RVE) in each “quadrature point” in the macroscale domain (possibly within a given timestep). Clearly, the purpose is to obtain macroscale properties of engineering interest; hence, whether it is possible to avoid resolution via DNS of the fine-scale problem and accept the homogenized solution can only be assessed via some sort of goal-oriented error quantification.

---

\* Corresponding author.

E-mail address: [emil.agggestam@chalmers.se](mailto:emil.agggestam@chalmers.se) (E. Aggestam).

However, it is widely realized that straight-forward application of the FE<sup>2</sup>-strategy can be computationally intractable for a fine macroscale mesh, particularly in 3D. Therefore, there is significant interest in reducing the cost of solving the individual RVE-problem(s) by introducing some kind of reduced basis, here denoted Numerical Model Reduction (NMR). In particular, we note strategies that are based on the superposition of “modes” that are characteristic for the RVE-solution fields. In the case of subscale small strain (visco)plasticity, various attempts have been made to approximate the inelastic strain field by a reduced basis, so called “inelastic modes”; one of the early proposals being the so called “eigendeformation-based reduced order homogenization” technique by Fish and coworkers, [1,2], which in its turn relies on the Transformation Field Analysis (TFA) that was originally proposed by Dvorak and Benveniste [3]. A similar approach, coined Nonuniform Transformation Field Analysis (NTFA), was proposed by Michel and Suquet [4,5]. Recent developments are by Fritzen and coworkers [6,7], who extended the idea further within the framework of Proper Orthogonal Decomposition (POD) and applied it to visco-elasticity and, more generally, to a (sub)class of Standard Dissipative Materials. Hernández et al. [8] proposed a reduced method based on POD and reduced sampling (quadrature) in a similar framework. Reduced order modeling in the context of the multiscale finite element model was considered by Nguyen [9]. Moreover, for a class of coupled problems an additional “bonus” is that it is possible to reduce the macroscale problem to that of a single-phase, whereby the “mode coefficients” play the role of classical internal variables, e.g. Jänicke et al. [10]. In other words, the character of homogenization problem changes such that the resulting macroscopic equations represent a single-phase poroviscoelastic material. Efendiev et al. [11] proposed a reduction basis from Spectral Decomposition in the context of porous media flow.

Quite importantly, however, is the obvious fact that the richness of the reduced basis will determine the accuracy of the RVE-solution, which calls for error control. An example of error estimation due to model reduction, although not in a homogenization context and for a PGD-basis, is Ladeveze and Chamoin [12]. PGD for homogenization of non-linear problems was considered by Cremonesi et al. [13]. Error estimators for POD-type reduction techniques have been developed by, e.g., Abdulle and Bai [14] for the heterogeneous multiscale method, Boyaval [15] and Paladim [16] for numerical homogenization, Ohlberger and Schindler [17] for the multiscale finite element method, and Kerfriden et al. [18] for projection-based reduced order modeling. Control of discretization errors (without model reduction) is discussed by, e.g., Jhurani and Demkowicz [19] and Larsson and Runesson [20].

In this paper, we consider the transient heat conduction as a model problem and choose, for simplicity, to use Spectral Decomposition to establish the reduced basis. (We consider the standard FE-solution in space–time as the exact one, i.e. we disregard any discretization error and consider only the error induced by the NMR strategy.) For this particular choice of basis, we discuss a few strategies to estimate the “solution error” without computing additional basis functions (modes). In particular, we aim for guaranteed, explicit bounds on the error in (i) energy norm and (ii) an arbitrary “quantity of interest” (QoI) within the realm of goal-oriented error estimation. It is noted that the QoI is generally defined in space–time to achieve maximal generality. As a “workhorse” for the error computation, that requires negligible additional cost, we thereby introduce an associated (non-physical) symmetrized variational problem in space–time and use ideas previously put forward by Parés et al. [21–23]. Furthermore, explicit bounds are obtained utilizing the discrete residual, cf. Jacobsson et al. [24] who developed bounds for Component Modal Synthesis (CMS) for static elasticity.

Throughout this paper, meager type is used to denote scalars, whereas bold type is used to denote vectors and (higher order) tensors. Scalar product (single contraction) is denoted by  $\cdot$ . For example, if  $\mathbf{a}$ ,  $\mathbf{b}$  are vectors and  $\mathbf{A}$  is a second order tensor, we have  $\mathbf{a} \cdot \mathbf{b} = a_i b_i$ ,  $(\mathbf{A} \cdot \mathbf{b})_i = A_{ij} b_j$ , where the Einstein summation convention is used.

As to homogenization in the spatial domain, volume averaging of an intensive field  $\diamond$  is denoted

$$\langle \diamond \rangle_{\square} \stackrel{\text{def}}{=} \frac{1}{|\Omega_{\square}|} \int_{\Omega_{\square}} \diamond d\Omega, \quad (1)$$

where  $\Omega_{\square}$  is the domain occupied by the RVE. The macroscale representation of  $\diamond$  is denoted  $\bar{\diamond}$ , and frequently it holds that  $\bar{\diamond} = \langle \diamond \rangle_{\square}$ .

The paper is organized as follows: Section 2 gives a review of computational homogenization as applied to the chosen transient model problem and introduces the concept of Numerical Model Reduction (NMR). Section 3 describes how to estimate the error from NMR. The error estimation is carried out both in the classical energy norm and in a relevant Quantity of Interest, e.g. time-averaged flux. Section 4 presents the numerical results that verify the performance of NMR and the quality of the derived explicit error estimates. The RVE is modeled in both one and three spatial dimensions. Finally, Section 5 concludes the paper with a summary and an outlook to future work.

## 2. Computational homogenization with model reduction

### 2.1. Definition of the model problem

Consider the transient heat flow problem on a fine scale in terms of the temperature field  $u(\mathbf{x}, t)$  that satisfies

$$\dot{\Phi}(u) + \nabla \cdot \mathbf{q}(\mathbf{g}[u]) = 0 \quad \text{in } \Omega \times (0, T], \tag{2a}$$

$$u = u^p(t) \quad \text{on } \Gamma_D \times (0, T], \tag{2b}$$

$$q_n \stackrel{\text{def}}{=} \mathbf{q} \cdot \mathbf{n} = q_n^p(t) \quad \text{on } \Gamma_N \times (0, T], \tag{2c}$$

$$\Phi = \Phi_0(\mathbf{x}) \quad \text{in } \Omega \text{ at } t = 0, \tag{2d}$$

where  $\Phi(u)$  is the volume-specific internal energy, and  $\mathbf{q}(\mathbf{g})$  is the heat flux field. We introduced the notation  $\mathbf{g}[u] \stackrel{\text{def}}{=} \nabla u$ , and a superposed dot for time-derivative (e.g.  $\dot{\Phi} = \frac{d\Phi}{dt}$ ). Standard Dirichlet and Neumann boundary conditions are introduced, i.e.  $\Gamma = \Gamma_D \cup \Gamma_N$ . For simplicity, the constitutive relations for  $\mathbf{q}$  and  $\Phi$  are chosen as linear and isotropic as

$$\mathbf{q}(\mathbf{g}[u]) = -k\mathbf{g}[u], \tag{3a}$$

$$\Phi(u) = cu, \tag{3b}$$

where  $k$  is the thermal conductivity and  $c$  is the volume-specific heat capacity. Hence, the initial condition (2d) is equivalent to  $u = u_0(\mathbf{x})$  at  $t = 0$ . Throughout the paper, both  $k = k(\mathbf{x})$  and  $c = c(\mathbf{x})$  may be strongly heterogeneous on the considered fine scale. The standard weak format in space corresponding to (2) and (3) reads: Find  $u(\bullet, t) \in \mathbb{U}(t)$  that solves

$$\mathfrak{m}(\dot{u}, \delta u) + \mathfrak{a}(u, \delta u) = \mathfrak{l}(t; \delta u) \quad \forall \delta u \in \mathbb{U}^0, \quad t \in (0, T], \tag{4a}$$

$$\mathfrak{m}(u(\bullet, 0), \delta u) = \mathfrak{m}(u_0, \delta u) \quad \forall \delta u \in \mathbb{U}^0, \tag{4b}$$

where we introduced the space-variational forms

$$\mathfrak{m}(u, \delta u) \stackrel{\text{def}}{=} \int_{\Omega} cu\delta u d\Omega, \tag{5a}$$

$$\mathfrak{a}(u, \delta u) \stackrel{\text{def}}{=} \int_{\Omega} k\mathbf{g}[\delta u] \cdot \mathbf{g}[u] d\Omega, \tag{5b}$$

$$\mathfrak{l}(t; \delta u) \stackrel{\text{def}}{=} - \int_{\Gamma_N} \delta u q_n^p(t) d\Gamma, \tag{5c}$$

and we define the standard function spaces

$$\mathbb{U}(t) = \{u \in \mathbb{H}^1(\Omega) : u = u^p(t) \text{ on } \Gamma_D\}, \tag{6a}$$

$$\mathbb{U}^0 = \{u \in \mathbb{H}^1(\Omega) : u = 0 \text{ on } \Gamma_D\}, \tag{6b}$$

where we note that the form  $\mathfrak{l}(t; \bullet)$ , as well as the trial space of spatial functions  $\mathbb{U}(t)$ , are parametrized with time due to possibly varying boundary conditions.

**Remark.**  $\mathbb{U}(t)$  defines the function space on  $\Omega$  and, therefore, a function  $u(\mathbf{x}, t)$  where  $u(\bullet, t) \in \mathbb{U}(t)$  is analytical in time.  $\square$

### 2.2. First order homogenization in the space domain

Rather than resolving the fine scale inherent in the solution of (4), we resort to variationally consistent homogenization on a Representative Volume Element (RVE), cf. Larsson et al. [25]. More specifically, we consider an RVE with size  $l_{\square}$ , which is centered at the spatial point  $\bar{\mathbf{x}} \in \Omega$  and occupies the domain  $\Omega_{\square}$ . The standard approach is then to decompose  $u$  into a macroscale part,  $u^M$ , and a microscale (or fluctuating) part,  $u^{\mu}$ , within each RVE. Hence,

$$u(\bar{\mathbf{x}}; \mathbf{x}, t) = u^M(\bar{\mathbf{x}}; \mathbf{x}, t) + u^{\mu}(\bar{\mathbf{x}}; \mathbf{x}, t), \tag{7}$$

where  $u^M$  is expressed in terms of the macroscale field  $\bar{u}$  as

$$u^M(\bar{\mathbf{x}}; \mathbf{x}, t) = \bar{u}(\bar{\mathbf{x}}, t) + \bar{\mathbf{g}}(\bar{\mathbf{x}}, t) \cdot [\mathbf{x} - \bar{\mathbf{x}}], \quad \bar{\mathbf{g}} \stackrel{\text{def}}{=} \mathbf{g}[\bar{u}] = \nabla \bar{u}. \tag{8}$$

The resulting macroscale problem in the space-variational format reads: Find  $\bar{u}(\bullet, t) \in \bar{\mathbb{U}}$  that solves<sup>1</sup>

$$\int_{\Omega} \left[ \dot{\bar{\Phi}} \delta \bar{u} + [\dot{\bar{\Phi}} - \bar{\mathbf{q}}] \cdot \mathbf{g}[\delta \bar{u}] \right] d\Omega = - \int_{\Gamma_N} \bar{q}_b^p(t) \delta \bar{u} d\Gamma \quad \forall \delta \bar{u} \in \bar{\mathbb{U}}^0, \tag{9}$$

subjected to the initial conditions

$$\bar{\Phi}(\bullet, 0) = \langle \Phi_0 \rangle_{\square} = \langle cu_0 \rangle_{\square}, \tag{10a}$$

$$\bar{\bar{\Phi}}(\bullet, 0) = \langle \Phi_0[\mathbf{x} - \bar{\mathbf{x}}] \rangle_{\square} = \langle cu_0[\mathbf{x} - \bar{\mathbf{x}}] \rangle_{\square}, \tag{10b}$$

where we introduced the macroscopic variables

$$\bar{\Phi} \stackrel{\text{def}}{=} \langle \Phi \rangle_{\square} = \langle cu \rangle_{\square}, \tag{11a}$$

$$\bar{\bar{\Phi}} \stackrel{\text{def}}{=} \langle \Phi[\mathbf{x} - \bar{\mathbf{x}}] \rangle_{\square} = \langle cu[\mathbf{x} - \bar{\mathbf{x}}] \rangle_{\square}, \tag{11b}$$

$$\bar{\mathbf{q}} \stackrel{\text{def}}{=} \langle \mathbf{q} \rangle_{\square} = \langle -k\mathbf{g}[u] \rangle_{\square}, \tag{11c}$$

and where we introduced the solution and test space  $\bar{\mathbb{U}}$  and  $\bar{\mathbb{U}}^0$ , respectively, in the appropriate fashion. In this context, the second order term  $\bar{\bar{\Phi}}$  may be denoted the ‘moment of heat content’ (similar to ‘moment of stresses’ in second-order homogenization) [25].

**Remark.** In this paper, brackets are used to denote operators, e.g.  $\mathbf{g}[\bar{u}]$ , while parentheses are used to denote standard algebraic functional dependence, e.g.  $u_0(\mathbf{x})$ .  $\square$

The purpose of the underlying RVE-problem, to be presented below, is to construct the implicit responses  $\bar{\Phi} = \Phi\{\bar{u}, \bar{\mathbf{g}}\}$ ,  $\bar{\bar{\Phi}} = \bar{\Phi}\{\bar{u}, \bar{\mathbf{g}}\}$  and  $\bar{\mathbf{q}} = \bar{\mathbf{q}}\{\bar{u}, \bar{\mathbf{g}}\}$ . Note, however, that the implicit relations depend on the full time history of the arguments. As to the appropriate formulation of the RVE-problem, we choose (for simplicity), homogeneous Dirichlet boundary conditions on  $u^\mu$ , i.e.  $u^\mu = 0$  on  $\Gamma_{\square}$ , see Fig. 1. We now consider the response of one single RVE located at  $\bar{\mathbf{x}}$ . Subsequently, we adopt the brief relation  $\bar{u}(\bar{\mathbf{x}}, t), \bar{\mathbf{g}}(\bar{\mathbf{x}}, t) \rightarrow \bar{u}(t), \bar{\mathbf{g}}(t)$ . Hence, the space-variational format of the RVE-problem reads: For given  $\bar{u}(t)$  and  $\bar{\mathbf{g}}(t)$ , find  $u^\mu(\bullet, t) \in \mathbb{U}_{\square}^0$  that solves

$$m_{\square}(\dot{u}^\mu, \delta u) + \alpha_{\square}(u^\mu, \delta u) = -m_{\square}(\dot{u}^M, \delta u) - \alpha_{\square}(u^M, \delta u) \quad \forall \delta u \in \mathbb{U}_{\square}^0, \quad t \in (0, T], \tag{12}$$

subjected to the initial condition

$$m_{\square}(u^\mu(\bullet, 0), \delta u) = m_{\square}(u_0 - u^M(\bullet, 0), \delta u) \quad \forall \delta u \in \mathbb{U}_{\square}^0, \tag{13}$$

where we introduced the bilinear forms

$$m_{\square}(u, \delta u) \stackrel{\text{def}}{=} \langle cu\delta u \rangle_{\square}, \tag{14a}$$

$$\alpha_{\square}(u, \delta u) \stackrel{\text{def}}{=} \langle \mathbf{g}[\delta u] \cdot k\mathbf{g}[u] \rangle_{\square}, \tag{14b}$$

and we define the RVE-spaces

$$\mathbb{U}_{\square}(t) = \{u \in \mathbb{H}^1(\Omega_{\square}) : u = \bar{u}(t) + \bar{\mathbf{g}}(t) \cdot [\mathbf{x} - \bar{\mathbf{x}}] \text{ on } \Gamma_{\square}\}, \tag{15a}$$

$$\mathbb{U}_{\square}^0 = \{u \in \mathbb{H}^1(\Omega_{\square}) : u = 0 \text{ on } \Gamma_{\square}\}. \tag{15b}$$

However, it turns out advantageous (for reasons that will be discussed later) to introduce, rather than (7), the alternative decomposition

$$u(\mathbf{x}, t) = u_{\text{stat}}\{\bar{u}(t), \bar{\mathbf{g}}(t)\}(\mathbf{x}) + \tilde{u}^\mu(\mathbf{x}, t), \tag{16}$$

where the time-dependent ‘‘stationary’’ field  $u_{\text{stat}}(\bullet, t) \in \mathbb{U}_{\square}(t)$  is the solution of

$$\alpha_{\square}(u_{\text{stat}}, \delta u) = 0 \quad \forall \delta u \in \mathbb{U}_{\square}^0, \quad t \in (0, T]. \tag{17}$$

<sup>1</sup> Here, the macroscale interpretation of the Neumann boundary condition defines  $q_n^p \rightarrow \bar{q}_n^p$ .

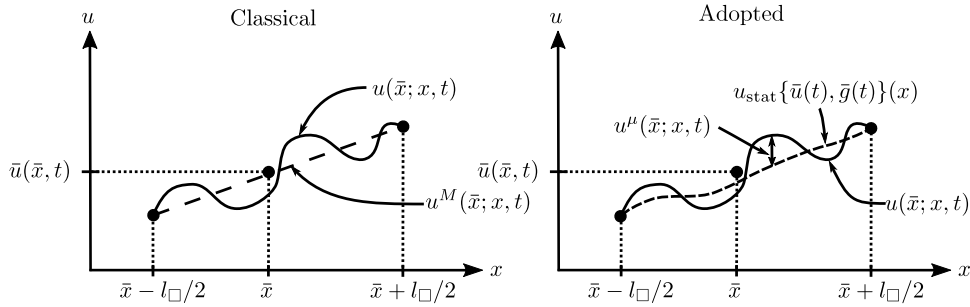


Fig. 1. Illustration of the difference between the classical and adopted approach in 1D.

In this paper, we exploit solely this decomposition; hence, the superimposed “~” on  $u^\mu$  is dropped subsequently. From (16) and (17) it follows that the RVE-problem, given in (12), can equivalently be formulated as: Find  $u^\mu(\bullet, t) \in \mathbb{U}_\square^0$  that satisfies the relation

$$m_\square(\dot{u}^\mu, \delta u) + a_\square(u^\mu, \delta u) = -m_\square(\dot{u}_{\text{stat}}, \delta u) \quad \forall \delta u \in \mathbb{U}_\square^0, \quad t \in (0, T], \tag{18}$$

subjected to the initial condition

$$m_\square(u^\mu(\bullet, 0), \delta u) = m_\square(u_0 - u_{\text{stat}}(\bullet, 0), \delta u) \quad \forall \delta u \in \mathbb{U}_\square^0. \tag{19}$$

Since (17) is a linear, elliptic problem for any given time  $t$  and since the boundary conditions on  $u_{\text{stat}}$  depend linearly on  $\bar{u}$  and  $\bar{g}(t)$ , we may conclude that  $u_{\text{stat}}$  depends linearly on  $\bar{u}$  and  $\bar{g}(t)$ , i.e. it is possible to compute sensitivity fields  $u_{\text{stat}}^{\mu(i)}(\mathbf{x}) \in \mathbb{U}_\square^0$  such that, following e.g. [26]

$$u_{\text{stat}} = \bar{u} + \sum_{i=1}^{n_{\text{dim}}} u_{\text{stat}}^{(i)} \mathbf{e}_i \cdot \bar{\mathbf{g}}(t), \tag{20}$$

where  $n_{\text{dim}}$  is the number of spatial dimensions,  $\{\mathbf{e}_i\}_{i=1}^{n_{\text{dim}}}$  are the set of orthonormal base vectors and

$$u_{\text{stat}}^{(i)} = [x_i - \bar{x}_i] + u_{\text{stat}}^{\mu(i)}, \quad \text{for } i = 1, 2, \dots, n_{\text{dim}}. \tag{21}$$

As a result, (18) can be rewritten as

$$m_\square(\dot{u}^\mu, \delta u) + a_\square(u^\mu, \delta u) = -m_\square(1, \delta u) \dot{\bar{u}}(t) - \sum_{i=1}^{n_{\text{dim}}} m_\square(u_{\text{stat}}^{(i)}, \delta u) \mathbf{e}_i \cdot \dot{\bar{\mathbf{g}}}(t) \quad \forall \delta u \in \mathbb{U}_\square^0, \quad t \in (0, T]. \tag{22}$$

It is noted that  $u_{\text{stat}}(\bullet, t) \in \mathbb{U}_\square$ , whereas  $u_{\text{stat}}^{\mu(i)}(\bullet, t) \in \mathbb{U}_\square^0$ .

### 2.3. Numerical Model Reduction (NMR)

As a preliminary, we consider  $\mathbb{U}_\square^0$  as infinite-dimensional, spanned by suitably chosen linearly independent global basis functions (fields),  $\{u_\alpha(\mathbf{x})\}_{\alpha=1}^\infty$ , i.e. any  $v \in \mathbb{U}_\square^0$  can be represented as

$$v(\mathbf{x}) = \sum_{\alpha=1}^\infty u_\alpha(\mathbf{x}) \zeta_\alpha, \quad \zeta_\alpha \in \mathbb{R}, \tag{23}$$

where  $\zeta_\alpha$  are coordinates. In this paper, we restrict our attention to the situation when  $\mathbb{U}_\square^0$  is finite-dimensional (due to FE-discretization in space) with  $\text{dim} = N$ , whereby  $\mathbb{U}_\square^0 = \text{Span}\{u_\alpha\}_{\alpha=1}^N$ . This means that each  $v \in \mathbb{U}_\square^0$  can be represented by (23) with  $\infty$  replaced by  $N$ . Since the FE-solution employing  $\mathbb{U}_\square^0$  is taken as the exact one, the discretization error will be disregarded in the subsequent error analysis (in this paper).

Next, we introduce “modal reduction” via  $\mathbb{U}_{\square, R}^0 = \text{Span}\{u_\alpha\}_{\alpha=1}^{N_R} \subset \mathbb{U}_{\square}^0$ , where  $N_R \ll N$ . We may thus approximate  $u^\mu$  as  $u_R^\mu$  with  $u_R^\mu(\bullet, t) \in \mathbb{U}_{\square, R}^0$

$$u^\mu(\mathbf{x}, t) \simeq u_R^\mu(\mathbf{x}, t) = \sum_{\alpha=1}^{N_R} u_\alpha(\mathbf{x})\xi_\alpha(t), \tag{24}$$

where  $\xi_\alpha$  are “mode activity” parameters. At a given time instance, we may thus define the trial set  $\mathbb{U}_{\square, R}(t)$  as follows:

$$\mathbb{U}_{\square, R}(t) = \{v \in \mathbb{U}_{\square}(t); v = u_{\text{stat}}(t) + v_R^\mu, v_R^\mu \in \mathbb{U}_{\square, R}^0\} \subset \mathbb{U}_{\square}(t). \tag{25}$$

Clearly, it is possible to choose the basis functions  $u_\alpha$  in many different ways. Since the considered RVE-problem is linear, the classical Spectral Decomposition method [27] is a viable choice. We thus compute the eigenpairs  $(u_\alpha, \lambda_\alpha) \in \mathbb{U}_{\square}^0 \otimes \mathbb{R}^+$  such that

$$a_{\square}(u_\alpha, \delta u) = \lambda_\alpha m_{\square}(u_\alpha, \delta u) \quad \forall \delta u \in \mathbb{U}_{\square}^0, \quad \alpha = 1, 2, \dots, N, \tag{26a}$$

$$m_{\square}(u_\alpha, u_\beta) = \delta_{\alpha\beta} \quad \alpha, \beta = 1, 2, \dots, N, \tag{26b}$$

with  $\lambda_1 \leq \lambda_2 \leq \dots \leq \lambda_N$ . Combining (26a) and (26b), we obtain the standard orthogonality condition

$$a_{\square}(u_\alpha, u_\beta) = \lambda_\alpha \delta_{\alpha\beta} \quad \alpha, \beta = 1, 2, \dots, N. \tag{27}$$

Upon inserting the expansion of  $u_R^\mu$  into (18) and (19), using the orthogonality conditions (26b) and (27), while choosing the test functions  $\delta u(\mathbf{x}) = u_\beta(\mathbf{x})\delta\zeta_\beta$  for arbitrary  $\delta\zeta_\beta \in \mathbb{R}, \beta = 1, 2, \dots, N_R$ , we obtain the diagonalized normal equations for the modal activity parameters  $\xi_\alpha(t)$  as follows:

$$\dot{\xi}_\alpha + \lambda_\alpha \xi_\alpha = f_\alpha(t), \quad \alpha = 1, 2, \dots, N_R, \tag{28a}$$

$$\xi_\alpha(0) = \xi_{\alpha,0} \stackrel{\text{def}}{=} m_{\square}(u_0 - u_{\text{stat}}(\bullet, 0), u_\alpha), \tag{28b}$$

where

$$f_\alpha(t) \stackrel{\text{def}}{=} -m_{\square}(\dot{u}_{\text{stat}}, u_\alpha) = f_{\bar{u}, \alpha} \dot{\bar{u}} + f_{\bar{g}, \alpha} \cdot \dot{\bar{g}}, \tag{29}$$

and

$$f_{\bar{u}, \alpha} \stackrel{\text{def}}{=} -m_{\square}(1, u_\alpha), \tag{30a}$$

$$f_{\bar{g}, \alpha} \stackrel{\text{def}}{=} -\sum_{i=1}^{n_{\text{dim}}} m_{\square}(u_{\text{stat}}^{(i)}, u_\alpha) \mathbf{e}_i. \tag{30b}$$

After integrating (28a) and (28b) to give  $\xi_\alpha(t)$ , we compute

$$u_R(\mathbf{x}, t) = u_{\text{stat}}\{\bar{u}(t), \bar{g}(t)\}(\mathbf{x}) + \sum_{\alpha=1}^{N_R} u_\alpha(\mathbf{x})\xi_\alpha(t). \tag{31}$$

Finally, the “effective” macroscale variables become

$$\bar{\Phi}(t) = \bar{\Phi}_{\bar{u}} \bar{u}(t) + \bar{\Phi}_{\bar{g}} \cdot \bar{g}(t) + \sum_{\alpha=1}^{N_R} \bar{\Phi}_{\alpha}^{\mu} \xi_\alpha(t), \tag{32a}$$

$$\bar{\bar{\Phi}}(t) = \bar{\bar{\Phi}}_{\bar{u}} \bar{u}(t) + \bar{\bar{\Phi}}_{\bar{g}} \cdot \bar{g}(t) + \sum_{\alpha=1}^{N_R} \bar{\bar{\Phi}}_{\alpha}^{\mu} \xi_\alpha(t), \tag{32b}$$

$$\bar{\bar{\bar{q}}}(t) = \bar{\bar{\bar{q}}}_{\bar{u}} \bar{u}(t) + \bar{\bar{\bar{q}}}_{\bar{g}} \cdot \bar{g}(t) + \sum_{\alpha=1}^{N_R} \bar{\bar{\bar{q}}}_{\alpha}^{\mu} \xi_\alpha(t), \tag{32c}$$

where

$$\bar{\Phi}_{\bar{u}} = c \quad \bar{\Phi}_{\bar{g}} = \sum_{i=1}^{n_{\text{dim}}} \langle cu_{\text{stat}}^{(i)} \rangle_{\square} \mathbf{e}_i \quad \bar{\Phi}_{\alpha}^{\mu} = \langle cu_{\alpha} \rangle_{\square}, \quad (33a)$$

$$\bar{\bar{\Phi}}_{\bar{u}} = \langle c[\mathbf{x} - \bar{\mathbf{x}}] \rangle_{\square} \quad \bar{\bar{\Phi}}_{\bar{g}} = \sum_{i=1}^{n_{\text{dim}}} \langle cu_{\text{stat}}^{(i)}[\mathbf{x} - \bar{\mathbf{x}}] \rangle_{\square} \otimes \mathbf{e}_i \quad \bar{\bar{\Phi}}_{\alpha}^{\mu} = \langle cu_{\alpha}[\mathbf{x} - \bar{\mathbf{x}}] \rangle_{\square}, \quad (33b)$$

$$\bar{q}_{\bar{u}} = \mathbf{0} \quad \bar{q}_{\bar{g}} = \sum_{i=1}^{n_{\text{dim}}} \langle -k \nabla u_{\text{stat}}^{(i)} \rangle_{\square} \otimes \mathbf{e}_i \quad \bar{q}_{\alpha}^{\mu} = \langle -k \nabla u_{\alpha} \rangle_{\square}. \quad (33c)$$

We note that  $\bar{\Phi}_{\bar{u}}$ ,  $\bar{\Phi}_{\alpha}^{\mu}$  are scalars,  $\bar{\Phi}_{\bar{g}}$ ,  $\bar{\bar{\Phi}}_{\bar{u}}$ ,  $\bar{\bar{\Phi}}_{\alpha}^{\mu}$ ,  $\bar{q}_{\bar{u}}$ ,  $\bar{q}_{\alpha}^{\mu}$  are vectors, and  $\bar{\bar{\Phi}}_{\bar{g}}$ ,  $\bar{q}_{\bar{g}}$  are second order tensors.

#### 2.4. Projection into NMR-space

We introduce the projection operator  $\Pi_R : \mathbb{L}_2(\Omega_{\square}) \rightarrow \mathbb{U}_{\square, R}^0$ , s.t., for any given  $v \in \mathbb{L}_2(\Omega_{\square})$ , the projection  $\Pi_R v$  is defined by the identity

$$\mathfrak{m}_{\square}(\Pi_R v, \delta u_R) = \mathfrak{m}_{\square}(v, \delta u_R) \quad \forall \delta u_R \in \mathbb{U}_{\square, R}^0. \quad (34)$$

Moreover, we introduce the orthogonal complement to  $\Pi_R$ , denoted  $\Pi_C = \mathbb{I} - \Pi_R$  s.t.  $\Pi_C v \in \mathbb{U}_{\square, C}^0 \stackrel{\text{def}}{=} \mathbb{U}_{\square}^0 \ominus \mathbb{U}_{\square, R}^0$ . It is then possible to conclude that, for any  $v \in \mathbb{U}_{\square}^0$ , we have the simple representation

$$v(\mathbf{x}) = \sum_{\alpha=1}^N u_{\alpha}(\mathbf{x}) \zeta_{\alpha}, \quad \Pi_R v(\mathbf{x}) = \sum_{\alpha=1}^{N_R} u_{\alpha}(\mathbf{x}) \zeta_{\alpha}, \quad \Pi_C v(\mathbf{x}) = \sum_{\alpha=N_R+1}^N u_{\alpha}(\mathbf{x}) \zeta_{\alpha}, \quad (35)$$

i.e.  $\Pi_R v$  is a direct truncation of  $v$ . From the orthogonality properties in (27)

$$\mathfrak{a}_{\square}(v, \delta u_R) = \mathfrak{a}_{\square}(\Pi_R v, \delta u_R), \quad \forall v, \delta u_R \in \mathbb{U}_{\square}^0 \times \mathbb{U}_{\square, R}^0. \quad (36)$$

**Remark.** For  $v \in \mathbb{U}_{\square}^0$ , the form  $\mathfrak{a}_{\square}(\bullet, \bullet)$  could have been used to define  $\Pi_R$ . However, in order to define  $\Pi_R$  on  $\mathbb{L}_2(\Omega_{\square})$ , we use the proposed definition in (34).  $\square$

For any given  $v_1, v_2 \in \mathbb{U}_{\square}^0$ , the following useful identities hold by definition of the projection operators:

$$\mathfrak{m}_{\square}(\Pi_R v_1, \Pi_C v_2) = \mathfrak{m}_{\square}(\Pi_C v_1, \Pi_R v_2) = 0, \quad (37a)$$

$$\mathfrak{m}_{\square}(v_1, \Pi_C v_2) = \mathfrak{m}_{\square}(\Pi_C v_1, \Pi_C v_2) = \mathfrak{m}_{\square}(\Pi_C v_1, v_2), \quad (37b)$$

$$\mathfrak{m}_{\square}(v_1, \Pi_R v_2) = \mathfrak{m}_{\square}(\Pi_R v_1, \Pi_R v_2) = \mathfrak{m}_{\square}(\Pi_R v_1, v_2). \quad (37c)$$

Completely equivalent identities hold for  $\mathfrak{a}_{\square}(v_1, v_2)$ , which follows from the representations in (35). In particular, we note that

$$\mathfrak{a}_{\square}(v_1, \Pi_C v_2) = \mathfrak{a}_{\square}(\Pi_C v_1, v_2). \quad (38)$$

Finally, we consider relations between the pertinent norms

$$\|\bullet\|_{\mathfrak{m}} \stackrel{\text{def}}{=} \sqrt{\mathfrak{m}_{\square}(\bullet, \bullet)}, \quad \|\bullet\|_{\mathfrak{a}} \stackrel{\text{def}}{=} \sqrt{\mathfrak{a}_{\square}(\bullet, \bullet)}. \quad (39)$$

Using (35), we obtain

$$\|\Pi_C v\|_{\mathfrak{m}}^2 = \sum_{\alpha=N_R+1}^N \zeta_{\alpha}^2, \quad \|\Pi_C v\|_{\mathfrak{a}}^2 = \sum_{\alpha=N_R+1}^N \lambda_{\alpha} \zeta_{\alpha}^2. \quad (40)$$

Since  $\lambda_1 \leq \lambda_2 \leq \dots \leq \lambda_N$ , it follows that

$$\|\Pi_C v\|_{\mathfrak{m}}^2 \leq \frac{1}{\lambda_{N_R}} \sum_{\alpha=N_R+1}^N \lambda_{\alpha} \zeta_{\alpha}^2 = \frac{1}{\lambda_{N_R}} \|\Pi_C v\|_{\mathfrak{a}}^2. \quad (41)$$

### 3. Error estimation in NMR

#### 3.1. Preliminaries

The aim of the error estimation is to assess the accuracy in predefined macroscopic quantities of interest, such as  $\bar{\Phi}(t)$  and  $\bar{q}(t)$  or suitable functionals thereof. In doing so, we first conclude that the total error involved in the computational results stem from different sources, viz. (i) space–time discretization (ii) NMR. In what follows, we ignore the discretization error. Recalling (16), we have

$$u = u_{\text{stat}}\{\bar{u}, \bar{g}\} + u^\mu, \quad u_R = u_{\text{stat}}\{\bar{u}, \bar{g}\} + u_R^\mu, \quad (42)$$

and we define the error

$$e(\mathbf{x}, t) \stackrel{\text{def}}{=} u(\mathbf{x}, t) - u_R(\mathbf{x}, t) = u^\mu(\mathbf{x}, t) - u_R^\mu(\mathbf{x}, t) = \sum_{\alpha=N_R+1}^N u_\alpha(\mathbf{x})\xi_\alpha(t). \quad (43)$$

Clearly, it is possible to compute this error exactly only if all modes  $\{u_\alpha\}_{\alpha=N_R+1}^N$  are computed in addition to those involved in the solution  $u_R^\mu$ ; however, this knowledge is of little use in practice since the computational cost would not be reduced as compared to the “brute force” solution of the FE-problem. Rather, in this paper we attempt at estimating the quality of the NMR-solution in terms of the effect of the error on a predefined “quantity of interest” without computing any additional modes than the  $N_R$  modes that span  $\mathbb{U}_{\square, R}^0$ . In fact, we shall aim for guaranteed, although not necessarily sharp, bounds of the Quantity of Interest,  $Q_\square(u)$ , for a given discretization. To this end, we base our estimate on the following “building blocks”:

- Abstract space–time formulation of the RVE-problem.
- Duality-based estimation of the error in  $Q_\square(u)$ .
- Construction of a symmetrized bilinear form in space–time, cf. [21].
- Explicit error estimate, cf. [24].

A brief summary of the key results is given in Section 3.8.

#### 3.2. Space–time weak format of the RVE-problem

The space–time weak format of the RVE-problem reads: Find  $u \in \mathcal{U}_\square$  such that<sup>2</sup>

$$A_\square(u, v) = L_\square(v) \quad \forall v \in \mathcal{V}_\square, \quad (44)$$

where we introduced the RVE-forms

$$A_\square(u, v) \stackrel{\text{def}}{=} \int_0^T [\mathfrak{m}_\square(\dot{u}, v) + \mathfrak{a}_\square(u, v)] dt + \mathfrak{m}_\square(u(\bullet, 0), v(\bullet, 0)), \quad (45a)$$

$$L_\square(v) \stackrel{\text{def}}{=} \mathfrak{m}_\square(u_0, v(\bullet, 0)), \quad (45b)$$

where  $\mathcal{U}_\square = \mathbb{H}^1([0, T]; \mathbb{U}_\square)$  and  $\mathcal{V}_\square$  is defined as

$$\mathcal{V}_\square = \{v(\mathbf{x}, t) : v(\bullet, 0) \in \mathbb{U}_\square^0, v|_{(0, T)} \in \mathbb{L}_2((0, T); \mathbb{U}_\square^0)\}. \quad (46)$$

We also introduce, (for later use)  $\mathcal{U}_\square^0 = \mathbb{H}^1([0, T]; \mathbb{U}_\square^0)$ . Here, we introduce the Bochner spaces

$$\mathbb{H}^1([0, T]; \mathbb{U}_\square^0) = \{v(\mathbf{x}, t), \|v(\bullet, t)\|_{\mathbb{U}_\square^0} = \|v(\bullet, t)\|_{\mathbb{H}^1(\Omega_\square)} \in \mathbb{H}^1([0, T])\}, \quad (47a)$$

$$\mathbb{L}_2((0, T); \mathbb{U}_\square^0) = \{v(\mathbf{x}, t), \|v(\bullet, t)\|_{\mathbb{U}_\square^0} = \|v(\bullet, t)\|_{\mathbb{H}^1(\Omega_\square)} \in \mathbb{L}_2([0, T])\}. \quad (47b)$$

We emphasize that the functions in  $\mathcal{U}_\square, \mathcal{U}_\square^0$  are defined at both  $t = 0$  and  $t = T$  and that  $\mathcal{U}_\square^0 \subset \mathcal{V}_\square$ , see Fig. 2.

The NMR-version of the RVE-problem reads: Find  $u_R \in \mathcal{U}_{\square, R} \subset \mathcal{U}_\square$  such that

$$A_\square(u_R, v_R) = L_\square(v_R) \quad \forall v_R \in \mathcal{V}_{\square, R} \subseteq \mathcal{V}_\square, \quad (48)$$

<sup>2</sup> Whereas  $\delta u \in \mathbb{U}_\square^0$  in (18) denotes a variation of  $u \in \mathbb{U}_\square$ , we here consider test functions belonging to different spaces for the non-symmetric space–time forms.

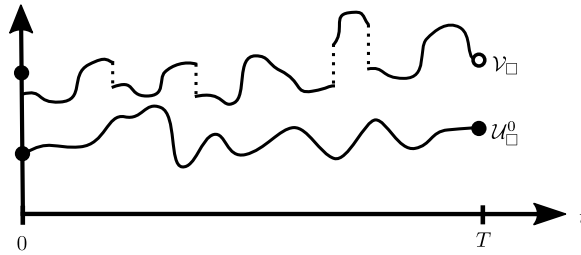


**Fig. 2.** Illustration in 1D of the difference between the spaces  $\mathcal{U}_{\square}^0$  and  $\mathcal{V}_{\square}$ . Functions in  $\mathcal{V}_{\square}$  are in  $\mathbb{L}_2((0, T))$  and can be evaluated pointwise at  $t = 0$ , but not at  $t = T$  (as indicated by “•” and “○”, respectively). Function in  $\mathcal{U}_{\square}^0$  has derivatives in  $\mathbb{L}_2((0, T))$  and can be evaluated at both  $t = 0$  and  $t = T$ .

where  $\mathcal{U}_{\square, R} = \mathbb{H}^1([0, T]; \mathbb{U}_{\square, R})$  and  $\mathcal{V}_{\square, R} = \{v(x, t) = v(\bullet, 0) \in \mathbb{U}_{\square, R}^0, v|_{(0, t)} \in \mathbb{L}_2((0, T); \mathbb{U}_{\square, R}^0)\}$ . Finally, we note that the space–time solution can be decomposed into

$$u_R = u_{\text{stat}}(x, t) + u_R^\mu, \tag{49}$$

with  $u_R^\mu \in \mathcal{U}_{\square, R}^0 = \mathbb{H}_1([0, T]; \mathbb{U}_{\square, R}^0)$ . As a result, (48) is completely equivalent to the set of equations (28a) and (28b).

### 3.3. Representation of quantity of interest

Before outlining the steps indicated above in further detail, we introduce a class of linear<sup>3</sup> goal functionals  $Q_{\square}(u)$ . It turns out advantageous, (for reasons that will be discussed later) to introduce the decomposition:

$$Q_{\square}(u) = Q_{\square}(u_{\text{stat}}) + Q_{\square}^0(u^\mu), \tag{50}$$

where, for a given  $Q_{\square}$ ,  $Q_{\square}^0$  must satisfy the identity

$$Q_{\square}^0(v) = Q_{\square}(v) \quad \forall v \in \mathcal{U}_{\square}^0. \tag{51}$$

Considering the constraint (51), we may introduce the following representation of  $Q_{\square}^0(v)$ :

$$Q_{\square}^0(v) \stackrel{\text{def}}{=} \int_0^T [\mathfrak{m}_{\square}(X, v) + \mathfrak{a}_{\square}(Y, v)] dt + \mathfrak{m}_{\square}(Z, v(\bullet, T)), \tag{52}$$

where  $X, Y \in \mathbb{L}_2((0, T), \mathbb{U}_{\square}^0)$ ,  $Z \in \mathbb{U}_{\square}^0$  are given (a priori chosen) functions. Due to the linearity of  $Q_{\square}^0$ , we have

$$\begin{aligned} E_Q &\stackrel{\text{def}}{=} Q_{\square}(u) - Q_{\square}(u_R) = Q_{\square}^0(u^\mu) - Q_{\square}^0(u_R^\mu) = Q_{\square}^0(e) \\ &= \int_0^T [\mathfrak{m}_{\square}(X, e) + \mathfrak{a}_{\square}(Y, e)] dt + \mathfrak{m}_{\square}(Z, e(\bullet, T)). \end{aligned} \tag{53}$$

Examples of  $Q_{\square}(u)$ , that will be adopted below for the numerical assessment, are:

#### Example 1: Time-average stored heat.

$$Q_{\square}(u) = \frac{1}{T} \int_0^T \bar{\Phi}(u) dt = \int_0^T \mathfrak{m}_{\square}\left(\frac{1}{T}, u\right) dt. \tag{54}$$

From (51), (52) and (54) follows that  $Y = Z = 0$ , whereas  $X \in \mathbb{U}_{\square}^0$  is determined from the weak identity

$$\mathfrak{m}_{\square}(X, \delta u) = \mathfrak{m}_{\square}\left(\frac{1}{T}, \delta u\right) \quad \forall \delta u \in \mathbb{U}_{\square}^0, \quad t \in (0, T). \tag{55}$$

#### Example 2: Time-average heat flux.

$$Q_{\square}(u) = \frac{1}{T} \int_0^T \bar{q} \cdot e_i dt = \int_0^T \mathfrak{a}_{\square}\left(-\frac{e_i \cdot [x - \bar{x}]}{T}, u\right) dt. \tag{56}$$

<sup>3</sup> Linearity is an essential property for the subsequent arguments.

From (51), (52) and (56) follows that  $X = Z = 0$ , whereas  $Y \in \mathbb{U}_\square^0$  is determined from the weak identity

$$\mathfrak{a}_\square(Y, \delta u) = \mathfrak{a}_\square\left(-\frac{\mathbf{e}_i \cdot [\mathbf{x} - \bar{\mathbf{x}}]}{T}, \delta u\right) \quad \forall \delta u \in \mathbb{U}_\square^0, \quad t \in (0, T]. \quad (57)$$

**Example 3: Stored heat at  $t = T$ .**

$$\mathcal{Q}_\square(u) = \bar{\Phi}(u(\bullet, T)) = \mathfrak{m}_\square(1, u(\bullet, T)). \quad (58)$$

From (51), (52) and (58) follows that  $X = Y = 0$ , whereas  $Z \in \mathbb{U}_\square^0$  is determined from the weak identity

$$\mathfrak{m}_\square(Z, \delta u) = \mathfrak{m}_\square(1, \delta u) \quad \forall \delta u \in \mathbb{U}_\square^0. \quad (59)$$

**Remark.** The solutions of (55) and (59) are obtained in practice (as is  $u_{\text{stat}}^{(i)}, i = 1, 2, \dots, n_{\text{dim}}$ ) via finite element discretization to a sufficient degree of accuracy by DNS. However, an explicit expression of the solution to (57) can be obtained as

$$Y = \frac{1}{T} [u_{\text{stat}}^{(i)} - \mathbf{e}_i \cdot [\mathbf{x} - \bar{\mathbf{x}}]] = \frac{1}{T} [u_{\text{stat}}^{(i)} - [x_i - \bar{x}_i]]. \quad (60)$$

Since  $u_{\text{stat}}^{(i)} = x_i - \bar{x}_i$  on  $\Gamma_\square$ , it is confirmed that  $Y = 0$  on  $\Gamma_\square$ , i.e.  $Y(\bullet, t) \in \mathbb{U}_\square^0$ .  $\square$

### 3.4. Error representation based on duality

From the bilinearity of  $A_\square(\bullet, \bullet)$ , we obtain the error equation for  $e = u - u_{\text{R}} \in \mathcal{U}_\square^0$

$$A_\square(e, v) = L_\square(v) - A_\square(u_{\text{R}}, v) \stackrel{\text{def}}{=} R_\square(v) \quad \forall v \in \mathcal{V}_\square. \quad (61)$$

In particular, using (48), we obtain the ‘‘Galerkin orthogonality’’,

$$R_\square(v_{\text{R}}) = 0 \quad \forall v_{\text{R}} \in \mathcal{V}_{\square, \text{R}}. \quad (62)$$

Next, we establish the dual problem. As a preliminary, we introduce the dual test space  $\mathcal{V}_\square^*$  as

$$\mathcal{V}_\square^* = \{v(\mathbf{x}, t) : v|_{(0, T)} \in \mathbb{L}_2((0, T); \mathbb{U}_\square^0), \quad v(\bullet, T) \in \mathbb{U}_\square^0\}, \quad (63)$$

and integrate by parts in  $A_\square$  to obtain

$$A_\square^*(u, v) = \int_0^T [-\mathfrak{m}_\square(\dot{u}, v) + \mathfrak{a}_\square(u, v)] dt + \mathfrak{m}_\square(u(\bullet, T), v(\bullet, T)), \quad (64)$$

where it was used that  $\mathfrak{m}_\square$  and  $\mathfrak{a}_\square$  are symmetric forms, and where it was tacitly assumed that  $u$  is ‘‘sufficiently’’ smooth in the time domain. The dual problem then reads: Find  $u^* \in \mathcal{U}_\square^0$  such that

$$A_\square^*(u^*, v) = \mathcal{Q}_\square^0(v) \quad \forall v \in \mathcal{V}_\square^*. \quad (65)$$

**Remark.** In the special case that  $v, w \in \mathcal{U}_\square^0$ , then  $A_\square(v, w) = A_\square^*(w, v)$ .  $\square$

Now, since  $\mathcal{U}_\square^0 \subset \mathcal{V}_\square^*$  and  $\mathcal{U}_\square^0 \subset \mathcal{V}_\square$ , we may combine (61) and (65) with the identity in the previous Remark to obtain the *exact* error representation

$$E_{\text{Q}} = \mathcal{Q}_\square^0(e) = A_\square^*(u^*, e) = A_\square(e, u^*) = R_\square(u^*). \quad (66)$$

Moreover, the Galerkin orthogonality in (62) gives  $R_\square(\Pi_{\text{R}} u^*) = 0$ , where we allow for the projection  $\Pi_{\text{R}} : \mathbb{U}_\square^0 \rightarrow \mathbb{U}_{\square, \text{R}}$  to extend naturally to space–time functions, since  $\Pi_{\text{R}} u^* \in \mathcal{U}_{\square, \text{R}}^0 \subset \mathcal{V}_{\square, \text{R}}$ . Combining this result with (66), we obtain

$$E_{\text{Q}} = R_\square(u^* - \Pi_{\text{R}} u^*). \quad (67)$$

We may also establish the NMR-version of the dual RVE-problem: Find  $u_{\text{R}}^* \in \mathcal{U}_{\square, \text{R}}^0$  such that

$$A_\square^*(u_{\text{R}}^*, v_{\text{R}}) = \mathcal{Q}_{\square, \text{R}}^0(v_{\text{R}}) \quad \forall v_{\text{R}} \in \mathcal{V}_{\square, \text{R}}^*, \quad (68)$$

and the corresponding error equation for  $e^* \stackrel{\text{def}}{=} u^* - u_R^* \in \mathcal{U}_\square^0$  becomes

$$A_\square^*(e^*, v) = Q_\square^0(v) - A_\square^*(u_R^*, v) \stackrel{\text{def}}{=} R_\square^*(v) \quad \forall v \in \mathcal{V}_\square^*. \tag{69}$$

Similarly as for the primal problem, we obtain the Galerkin orthogonality

$$R_\square^*(v_R) = 0 \quad \forall v_R \in \mathcal{V}_{\square,R}^*. \tag{70}$$

### 3.5. Error estimation based on symmetrized problem

In order to establish (upper and lower) bounds on the error  $E_Q$ , it is useful to establish an “energy norm” that can be associated with the time-dependent RVE-problem given in (44). To this end, we exploit the idea proposed by [21] [in the context of the non-symmetric (non-selfadjoint) stationary diffusion–convection problem]. Since  $A_\square(\bullet, \bullet)$  is bilinear (but unsymmetrical), it is possible to construct the symmetric counterpart, denoted  $A_\square^s(\bullet, \bullet)$ , as follows:

$$A_\square^s(u, v) \stackrel{\text{def}}{=} \frac{1}{2} [A_\square(u, v) + A_\square^*(u, v)] = \int_0^T a_\square(u, v) dt + \frac{1}{2} m_\square(u(\bullet, 0), v(\bullet, 0)) + \frac{1}{2} m_\square(u(\bullet, T), v(\bullet, T)), \tag{71}$$

for  $u, v \in \mathcal{U}_\square^0$ . Next, we introduce the “symmetric” space  $\mathcal{V}_\square^s$

$$\mathcal{V}_\square^s = \{v(x, t) : v(\bullet, 0) \in \mathbb{U}_\square^0, v|_{(0,T)} \in \mathbb{L}_2((0, T); \mathbb{U}_\square^0), v(\bullet, T) \in \mathbb{U}_\square^0\}, \tag{72}$$

and we note that  $A_\square^s(v, w), R_\square(v), R_\square^*(v)$  are computable for  $v, w \in \mathcal{V}_\square^s$ . In addition to the Bochner space defined in (47), we note that functions in  $\mathcal{V}_\square^s$  have distinct components in  $t = 0$  and  $t = T$ .

Since  $A_\square^s(v, v)$  is coercive, we may define the energy norm on  $\mathcal{V}_\square^s$

$$\|v\| \stackrel{\text{def}}{=} \sqrt{A_\square^s(v, v)}. \tag{73}$$

Since  $\mathcal{U}_\square^0 \subset \mathcal{V}_\square^0$ , we note that the introduced norm is also a norm for functions in  $\mathcal{U}_\square^0$ . In practice, for  $e \in \mathcal{U}_\square^0$ , we can identify the identity

$$\|e\|^2 = A_\square^s(e, e) = A_\square(e, e), \tag{74}$$

following from (71). By using the  $\|\bullet\|_a$  and  $\|\bullet\|_m$  norms, introduced in (39), we may rewrite  $\|v\|$  more explicitly as

$$\|v\| = \left[ \int_0^T \|v\|_a^2 dt + \frac{1}{2} \|v(\bullet, 0)\|_m^2 + \frac{1}{2} \|v(\bullet, T)\|_m^2 \right]^{1/2}. \tag{75}$$

We may now introduce the “symmetrized error equation” for  $e^s \in \mathcal{V}_\square^s$ :

$$A_\square^s(e^s, v) = R_\square(v) \quad \forall v \in \mathcal{V}_\square^s. \tag{76}$$

It follows that, using the Cauchy–Schwarz inequality,

$$\|e\|^2 \stackrel{(74)}{=} A_\square(e, e) \stackrel{(61)}{=} R_\square(e) \stackrel{(76)}{=} A_\square^s(e^s, e) \leq \|e^s\| \|e\|, \tag{77}$$

and, hence,

$$E \stackrel{\text{def}}{=} \|e\| \leq \|e^s\|, \tag{78}$$

which is the basic estimate in the energy norm.

In complete analogy with (76), we introduce the symmetrized error equation associated with the dual problem (68), from which  $e^{*s} \in \mathcal{V}_\square^s$  can be solved:

$$A_\square^s(e^{*s}, v) = R_\square^*(v) \quad \forall v \in \mathcal{V}_\square^s, \tag{79}$$

and, by arguments that are similar to those leading to (78), it follows that

$$\|e^*\| \leq \|e^{*s}\|. \tag{80}$$

**Remark.** To capture the error transport in space–time, the symmetrized version is needed. Furthermore, this framework allows for further extensions of the theory that includes discretization error in addition to the NMR-error.  $\square$

**Remark.** The new error functions  $e^s$  and  $e^{*s}$  are defined entirely via their respective error equation that exploits the operator  $A_{\square}^s(\bullet, \bullet)$ . Although possible, there is no need to interpret  $e^s$  and  $e^{*s}$  as “errors” in any (actual or virtual) fields,  $u^s$  and  $u^{*s}$ , respectively.  $\square$

In order to obtain guaranteed bounds on  $E_Q$  (for a given discretization), we consider the following estimate:

**Theorem 1.** Let  $e^s$  be the solution of (76), whereas  $e^{*s}$  is the solution of (79) and  $\kappa \neq 0$  is an arbitrary constant, then

$$E_Q^- \stackrel{\text{def}}{=} -\frac{1}{4} \min_{\kappa \neq 0} \|\kappa e^s - \frac{1}{\kappa} e^{*s}\|^2 \leq E_Q \leq \frac{1}{4} \min_{\kappa \neq 0} \|\kappa e^s + \frac{1}{\kappa} e^{*s}\|^2 \stackrel{\text{def}}{=} E_Q^+. \quad (81)$$

**Proof.** Consider the inequality

$$0 \leq \left\| \frac{1}{2} \left[ \kappa e^s \pm \frac{1}{\kappa} e^{*s} \right] - \kappa e \right\|^2 = \frac{1}{4} \|\kappa e^s \pm \frac{1}{\kappa} e^{*s}\|^2 - \kappa^2 A_{\square}^s(e^s, e) \mp A_{\square}^s(e^{*s}, e) + \kappa^2 \|e\|^2. \quad (82)$$

From the error equation for the symmetric and non-symmetric problems it follows that

$$A_{\square}^s(e^s, e) = R_{\square}(e) = A_{\square}(e, e) = A_{\square}^s(e, e) = \|e\|^2. \quad (83)$$

Hence, the inequality in (82) can be simplified as

$$0 \leq \frac{1}{4} \|\kappa e^s \pm \frac{1}{\kappa} e^{*s}\|^2 \mp A_{\square}^s(e^{*s}, e). \quad (84)$$

The error equation from the dual symmetric problem and the definition of the dual residual give

$$A_{\square}^s(e^{*s}, e) = A_{\square}^s(e, e^{*s}) = R_{\square}^*(e) = Q_{\square}^0(e) - A_{\square}(e, u_R^*). \quad (85)$$

However, since  $u_R^* \in \mathcal{U}_{\square, R}^0$  it follows from the Galerkin orthogonality that

$$A_{\square}(e, u_R^*) = R_{\square}(u_R^*) = 0, \quad (86)$$

and, therefore, (85) simplifies to

$$A_{\square}^s(e^{*s}, e) = Q_{\square}^0(e) = E_Q. \quad (87)$$

Thus, (84) can be rewritten as

$$0 \leq \frac{1}{4} \|\kappa e^s \pm \frac{1}{\kappa} e^{*s}\|^2 \mp E_Q, \quad (88)$$

which is equivalent to

$$-\frac{1}{4} \|\kappa e^s - \frac{1}{\kappa} e^{*s}\|^2 \leq E_Q \leq \frac{1}{4} \|\kappa e^s + \frac{1}{\kappa} e^{*s}\|^2. \quad (89)$$

Since (89) is valid for arbitrary  $\kappa \neq 0$ , (81) follows.  $\square$

At this point it is worth noting that it is possible to compute the bounds  $E_Q^+$  and  $E_Q^-$  by solving for  $e^s$  and  $e^{*s}$  from the “symmetrized” error equations (76) and (79), respectively, to any degree of accuracy (even exactly). However, to do so would mean to involve more modes; the exact solution would require all  $N$  modes.<sup>4</sup> These error equations are “stationary” in character, i.e. no time derivative is involved, and thus much less expensive than the original error equations for  $e$  and  $e^*$  defined by (61) and (69), respectively. However, they still incur a considerable computational effort since they would require either the solution of eigenvalue problems to obtain the higher modes or the solution of a large number of stationary DNS problems pertaining to each time instance/quadrature point.

<sup>4</sup> The algorithms for computing  $e^s$  and  $e^{*s}$  exactly are given in Appendix A.

As a consequence we shall, therefore, aim at finding  $E_{Q,\text{est}}^- < 0$  and  $E_{Q,\text{est}}^+ > 0$  that make explicit use only of the given data and the reduced set of eigenpairs  $(u_\alpha, \lambda_\alpha)$  for  $\alpha = 1, 2, \dots, N_R$  such that the result in (81) can be bounded as

$$E_{Q,\text{est}}^- \leq E_Q^- \leq E_Q \leq E_Q^+ \leq E_{Q,\text{est}}^+ \tag{90}$$

It turns out that this can be achieved via further consideration of the solutions  $e^s$  and  $e^{*s}$  of the (primary) problem in (76) and the (dual) problem in (79), respectively. In order to do so, we first establish and analyze a generic problem (that comprises the two above-mentioned as special cases), as discussed in the next subsection.

### 3.6. Explicit error bounds — generic error equation

Consider the following generic RVE-problem: Find  $\chi \in \mathcal{V}_\square^s$  such that

$$A_\square^s(\chi, v) = \tilde{R}_\square(v) \quad \forall v \in \mathcal{V}_\square^s, \tag{91}$$

where  $A_\square^s(u, v)$  was given in (71), i.e.

$$A_\square^s(\chi, v) = \int_0^T a_\square(\chi, v) dt + \frac{1}{2} m_\square(\chi(\bullet, 0), v(\bullet, 0)) + \frac{1}{2} m_\square(\chi(\bullet, T), v(\bullet, T)), \tag{92}$$

whereas  $\tilde{R}_\square(v)$  is given by

$$\tilde{R}_\square(v) = \int_0^T [m_\square(A, v) + a_\square(B, v)] dt + m_\square(C, v(\bullet, 0)) + m_\square(D, v(\bullet, T)), \tag{93}$$

where  $A \in \mathbb{L}_2((0, T); \mathbb{L}_2(\Omega_\square))$ ,  $B \in \mathbb{L}_2((0, T); \mathbb{H}_1(\Omega_\square))$ ,  $C, D \in \mathbb{L}_2(\Omega_\square)$ . Furthermore, we shall assume that  $\tilde{R}_\square$  has the property

$$\tilde{R}_\square(v_R) = 0 \quad \forall v_R \in \mathcal{V}_{\square,R}^s, \tag{94}$$

where  $\mathcal{V}_{\square,R}^s$  is the restriction of  $\mathcal{V}_\square^s$  in (72) for  $\mathbb{U}_\square^0 \rightarrow \mathbb{U}_{\square,R}^0$ . Indeed, this corresponds to the orthogonalities in (62) and (70). As a consequence of (94),

$$\tilde{R}_\square(\Pi_R v) = 0 \quad \forall v \in \mathcal{V}_\square^s, \tag{95}$$

where we recall that the projection  $\Pi_R$  was introduced in (34). Moreover, recalling the complementary projection  $\Pi_C = \mathbb{I} - \Pi_R$ , we may rewrite  $\tilde{R}_\square(v)$  as

$$\tilde{R}_\square(v) = \tilde{R}_\square(\Pi_C v) = \int_0^T [m_\square(\Pi_C A, v) + a_\square(\Pi_C B, v)] dt + m_\square(\Pi_C C, v(\bullet, 0)) + m_\square(\Pi_C D, v(\bullet, T)), \tag{96}$$

where the last equality follows from (37) and (38). With (92) and (96), we conclude that (91) can be rewritten as follows:

$$a_\square(\chi, \delta u) = m_\square(\Pi_C A, \delta u) + a_\square(\Pi_C B, \delta u) \quad \forall \delta u \in \mathbb{U}_\square^0, \quad t \in (0, T), \tag{97a}$$

$$m_\square(\chi(\bullet, 0), \delta u) = m_\square(2\Pi_C C, \delta u) \quad \forall \delta u \in \mathbb{U}_\square^0, \tag{97b}$$

$$m_\square(\chi(\bullet, T), \delta u) = m_\square(2\Pi_C D, \delta u) \quad \forall \delta u \in \mathbb{U}_\square^0. \tag{97c}$$

Since  $m_\square(\Pi_C A, \delta u_R) = a_\square(\Pi_C B, \delta u_R) = 0$  for any  $\delta u_R \in \mathbb{U}_{\square,R}^0$ , it follows from (97a) that

$$a_\square(\chi, \delta u_R) = 0 \quad \forall \delta u_R \in \mathbb{U}_{\square,R}^0. \tag{98}$$

Consequently, following (36),  $\Pi_R \chi = 0$  and  $\Pi_C \chi = \chi$ .

In order to estimate  $\|\chi\|$ , we need to estimate  $\|\chi\|_a$ ,  $\|\chi(\bullet, 0)\|_m$  and  $\|\chi(\bullet, T)\|_m$  in terms of the given data, i.e. expressed in terms of  $A, B, C, D$ . The result is given in the following Theorem:

**Theorem 2.** *If  $\chi$  is the solution to (91), and thus (97), then it holds that*

$$\|\chi\|_a \leq \frac{\|\Pi_C A\|_m}{\sqrt{\lambda_{N_R}}} + \|\Pi_C B\|_a \quad \forall t \in (0, T), \tag{99}$$

and

$$\|\chi(\bullet, 0)\|_m \leq \|2\Pi_C C\|_m, \quad (100a)$$

$$\|\chi(\bullet, T)\|_m \leq \|2\Pi_C D\|_m, \quad (100b)$$

whereby we obtain

$$\|\chi\| \leq \left[ \int_0^T \left[ \frac{\|\Pi_C A\|_m}{\sqrt{\lambda_{N_R}}} + \|\Pi_C B\|_a \right]^2 dt + 2\|\Pi_C C\|_m^2 + 2\|\Pi_C D\|_m^2 \right]^{1/2}. \quad (101)$$

**Proof.** We first prove (99). Setting  $\delta u = \chi$  in (97), noting the identity  $m_\square(\Pi_C A, \chi) = m_\square(\Pi_C A, \Pi_C \chi)$  and applying Cauchy–Schwarz inequality, we obtain

$$\begin{aligned} \|\chi\|_a^2 &= a_\square(\chi, \chi) = m_\square(\Pi_C A, \Pi_C \chi) + a_\square(\Pi_C B, \chi) \leq \|\Pi_C A\|_m \|\Pi_C \chi\|_m \\ &\quad + \|\Pi_C B\|_a \|\chi\|_a \quad \forall t \in (0, T). \end{aligned} \quad (102)$$

Inserting the relation between the  $a$ -norm and  $m$ -norm in (41), i.e.

$$\|\Pi_C \chi\|_m^2 \leq \frac{1}{\lambda_{N_R}} \|\Pi_C \chi\|_a^2, \quad (103)$$

into (102), we obtain

$$\|\chi\|_a^2 \leq \|\Pi_C A\|_m \frac{\|\Pi_C \chi\|_a}{\sqrt{\lambda_{N_R}}} + \|\Pi_C B\|_a \|\chi\|_a = \|\Pi_C A\|_m \frac{\|\chi\|_a}{\sqrt{\lambda_{N_R}}} + \|\Pi_C B\|_a \|\chi\|_a \quad \forall t \in (0, T), \quad (104)$$

where it was used that  $\chi = \Pi_C \chi$ , cf. the discussion following (98). Finally, dividing by  $\|\chi\|_a$  in (104) we obtain (99). [Note that (99) and (100) are fulfilled in the trivial case when  $\|\chi\|_a = \|\chi(\bullet, 0)\|_m = \|\chi(\bullet, T)\|_m = 0$  since all norms are non-negative and  $\lambda_{N_R}$  is positive.]

In order to prove (100a), consider Eq. (97b), i.e.

$$m_\square(\chi(\bullet, 0), \delta u(\bullet, 0)) = m_\square(2\Pi_C C, \delta u(\bullet, 0)) \quad \forall \delta u \in \mathbb{U}_\square^0. \quad (105)$$

Setting  $\delta u(\bullet, 0) = \chi(\bullet, 0)$  and applying Cauchy–Schwarz inequality gives

$$\|\chi(\bullet, 0)\|_m^2 = m_\square(\chi(\bullet, 0), \chi(\bullet, 0)) = m_\square(2\Pi_C C, \chi(\bullet, 0)) \leq \|2\Pi_C C\|_m \|\chi(\bullet, 0)\|_m, \quad (106)$$

which implies that

$$\|\chi(\bullet, 0)\|_m \leq \|2\Pi_C C\|_m. \quad (107)$$

From the same argumentation, (100b) follows from (97c).

Finally, (75) gives

$$\|\chi\| = \left[ \int_0^T \|\chi\|_a^2 dt + \frac{1}{2} \|\chi(\bullet, 0)\|_m^2 + \frac{1}{2} \|\chi(\bullet, T)\|_m^2 \right]^{1/2}. \quad (108)$$

Combining (108) with the relations (99) and (100a) and (100b), we conclude the proof.  $\square$

Next, we may use the estimate in (101) by choosing  $\chi$  appropriately in order to obtain explicit expressions for  $E_{Q,\text{est}}^-$  and  $E_{Q,\text{est}}^+$ . However, in order to do so, we shall first establish estimates for  $\|e^s\|$  and  $\|e^{*s}\|$  by considering the primal and dual error equations, respectively.

### 3.7. Application of the generic error equation

#### 3.7.1. Symmetrized primary problem

The symmetrized version of the primal error equation (76) is retrieved from (91) if we choose  $\chi = e^s$  and  $\tilde{R}_\square = R_\square$ . Using (45a), (45b), we first note that  $R_\square(v)$  can be written as

$$\begin{aligned} R_\square(v) &= - \int_0^T [m_\square(\dot{u}_{\text{stat}} + \dot{u}_R^\mu, v) + a_\square(u_R^\mu, v)] dt \\ &\quad + m_\square(u_0 - u_{\text{stat}}(\bullet, 0) - u_R^\mu(\bullet, 0), v(\bullet, 0)) \quad \forall v \in \mathcal{V}_\square^s. \end{aligned} \quad (109)$$

However, using the Galerkin-orthogonality and the same arguments as in Section 3.6, we conclude that  $R_{\square}(v)$  can be further reduced to

$$R_{\square}(v) = - \int_0^T m_{\square}(\Pi_C \dot{u}_{\text{stat}}, v) dt + m_{\square}(\Pi_C(u_0 - u_{\text{stat}}(\bullet, 0)), v(\bullet, 0)), \tag{110}$$

where it was used that  $\Pi_C u_R^{\mu} = 0$ ,  $\Pi_C u_R^{\mu} = 0$ . For example, since  $\Pi_R u_R^{\mu} = u_R^{\mu}$ , it follows that  $\Pi_C u_R^{\mu} = 0$ . Identifying terms in (110) with the generic expression in (96), we obtain

$$\begin{cases} \Pi_C A = -\Pi_C \dot{u}_{\text{stat}}, \\ \Pi_C B = 0, \\ \Pi_C C = \Pi_C(u_0 - u_{\text{stat}}(\bullet, 0)), \\ \Pi_C D = 0. \end{cases} \tag{111}$$

Hence, we obtain from (101)

$$\|e^s\| \leq \left[ \int_0^T \frac{\|\Pi_C \dot{u}_{\text{stat}}\|_m^2}{\lambda_{NR}} dt + 2\|\Pi_C(u_0 - u_{\text{stat}}(\bullet, 0))\|_m^2 \right]^{1/2} \stackrel{\text{def}}{=} E_{\text{est}}^s. \tag{112}$$

**Remark.** As an intermediate result, we have obtained an explicit estimate of the energy norm of the error, i.e.

$$E \stackrel{\text{def}}{=} \|e\| \leq E_{\text{est}}^s, \tag{113}$$

where  $E_{\text{est}}^s$  was given in (112).  $\square$

### 3.7.2. Symmetrized dual problem

The symmetrized version of the dual error equation (79) is retrieved if we choose  $\chi = e^{*s}$  and  $\tilde{R}_{\square} = R_{\square}^*$ . Again, we may use the Galerkin-orthogonality to obtain

$$R_{\square}^*(v) = \int_0^T [m_{\square}(\Pi_C X, v) + a_{\square}(\Pi_C Y, v)] dt + m_{\square}(\Pi_C Z, v(\bullet, T)). \tag{114}$$

Identifying terms in (114) with the generic expression in (96), we obtain

$$\begin{cases} \Pi_C A = \Pi_C X, \\ \Pi_C B = \Pi_C Y, \\ \Pi_C C = 0, \\ \Pi_C D = \Pi_C Z, \end{cases} \tag{115}$$

and, thus,

$$\|e^{*s}\| \leq \left[ \int_0^T \left[ \frac{\|\Pi_C X\|_m}{\sqrt{\lambda_{NR}}} + \|\Pi_C Y\|_a \right]^2 dt + 2\|\Pi_C Z\|_m^2 \right]^{1/2} \stackrel{\text{def}}{=} E_{\text{est}}^{*s}. \tag{116}$$

### 3.7.3. Explicit error estimate in a quantity of interest

Finally, we aim at obtaining an explicit estimate of the upper and lower bounds on  $E_Q$  in (90), expressed as  $E_{Q,\text{est}}^+$  and  $E_{Q,\text{est}}^-$ , respectively. We then choose  $\chi = \kappa e^s \pm \frac{1}{\kappa} e^{*s}$  and  $\tilde{R}_{\square}(v) = \kappa R_{\square}(v) \pm \frac{1}{\kappa} R_{\square}^*(v)$ , whereafter we may directly use the results (111) and (115) to obtain

$$\begin{cases} \Pi_C A = -\kappa \Pi_C \dot{u}_{\text{stat}} \pm \frac{1}{\kappa} \Pi_C X, \\ \Pi_C B = \pm \frac{1}{\kappa} \Pi_C Y, \\ \Pi_C C = \kappa \Pi_C(u_0 - u_{\text{stat}}(\bullet, 0)), \\ \Pi_C D = \pm \frac{1}{\kappa} \Pi_C Z. \end{cases} \tag{117}$$

Hence, upon inserting into (101) we obtain

$$E_{Q,\text{est}}^+ = \frac{1}{4} \min_{\kappa \neq 0} \left[ \int_0^T \left[ \frac{\| -\kappa \Pi_C \dot{u}_{\text{stat}} + \frac{1}{\kappa} \Pi_C X \|_{\text{m}}}{\sqrt{\lambda_{N_R}}} + \left\| \frac{1}{\kappa} \Pi_C Y \right\|_{\alpha} \right]^2 dt + 2 \left\| \kappa \Pi_C (u_0 - u_{\text{stat}}(\bullet, 0)) \right\|_{\text{m}}^2 + 2 \left\| \frac{1}{\kappa} \Pi_C Z \right\|_{\text{m}}^2 \right]^{1/2}, \tag{118a}$$

$$E_{Q,\text{est}}^- = -\frac{1}{4} \min_{\kappa \neq 0} \left[ \int_0^T \left[ \frac{\| -\kappa \Pi_C \dot{u}_{\text{stat}} - \frac{1}{\kappa} \Pi_C X \|_{\text{m}}}{\sqrt{\lambda_{N_R}}} + \left\| \frac{1}{\kappa} \Pi_C Y \right\|_{\alpha} \right]^2 dt + 2 \left\| \kappa \Pi_C (u_0 - u_{\text{stat}}(\bullet, 0)) \right\|_{\text{m}}^2 + 2 \left\| \frac{1}{\kappa} \Pi_C Z \right\|_{\text{m}}^2 \right]^{1/2}. \tag{118b}$$

The values of  $\kappa$ , denoted  $\kappa^+$  and  $\kappa^-$  and which give the sharpest possible bounds, can be obtained numerically in the general case. However, in a few special cases the solutions can be obtained explicitly, as shown in Section 4.4.

**Remark.** The complementary projection is calculated as

$$\Pi_C y = y - \sum_{\alpha=1}^{N_R} \mathbf{m}_{\square}(y, u_{\alpha}) u_{\alpha}, \tag{119}$$

for any  $y \in \mathbb{U}_{\square}$ .  $\square$

### 3.8. Summary

A summary of the key results is given below.

1. The error equation, defined in (44), is given by

$$e \in \mathcal{U}_{\square}^0 : A_{\square}(e, v) = R_{\square}(v) \quad \forall v \in \mathcal{V}_{\square}.$$

2. The dual problem, defined in (65), and the dual error equation, defined in (69), are given by

$$u^* \in \mathcal{U}_{\square}^0 : A_{\square}^*(u^*, v) = Q_{\square}^0(v) \quad \forall v \in \mathcal{V}_{\square}^*,$$

$$e^* \in \mathcal{U}_{\square}^0 : A_{\square}^*(e^*, v) = R_{\square}^*(v) \quad \forall v \in \mathcal{V}_{\square}^*.$$

3. The symmetric counterpart of  $A_{\square}(\bullet, \bullet)$ , denoted  $A_{\square}^s(\bullet, \bullet)$ , is defined in (71) and is used to define the energy norm, see (73), as

$$\|v\| \stackrel{\text{def}}{=} \sqrt{A_{\square}^s(v, v)}, \quad \forall v \in \mathcal{V}_{\square}^s,$$

where

$$A_{\square}^s(u, v) \stackrel{\text{def}}{=} \frac{1}{2} [A_{\square}(u, v) + A_{\square}^*(u, v)], \quad \forall u, v \in \mathcal{U}_{\square}^0.$$

4. The symmetrized error equation, defined in (76), and the corresponding dual symmetrized error equation, defined in (79), are given by

$$e^s \in \mathcal{V}_{\square}^s : A_{\square}^s(e^s, v) = R_{\square}(v) \quad \forall v \in \mathcal{V}_{\square}^s,$$

$$e^{*s} \in \mathcal{V}_{\square}^s : A_{\square}^s(e^{*s}, v) = R_{\square}^*(v) \quad \forall v \in \mathcal{V}_{\square}^s.$$

5. With the parallelogram law, the symmetrized error equations are used to obtain bounds for the error in a quantity of interest, see (81), as

$$-\frac{1}{4} \min_{\kappa \neq 0} \left\| \kappa e^s - \frac{1}{\kappa} e^{*s} \right\|^2 \leq E_Q \leq \frac{1}{4} \min_{\kappa \neq 0} \left\| \kappa e^s + \frac{1}{\kappa} e^{*s} \right\|^2.$$

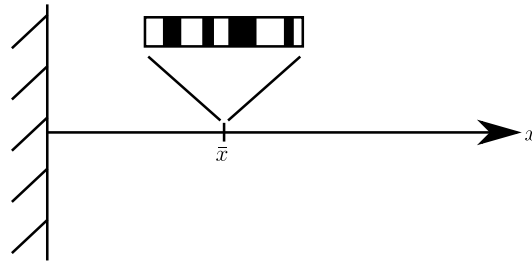


Fig. 3. Illustration of the coupling between the macro- and micro-scale problems used to define  $\bar{u}$  and  $\bar{g}$ .

6. By using the generic RVE-problem, defined in (91),

$$\kappa e^s \pm \frac{1}{\kappa} e^{*s} \in \mathcal{V}_\square^s : \quad A_\square^s \left( \kappa e^s \pm \frac{1}{\kappa} e^{*s}, v \right) = \kappa R_\square(v) \pm \frac{1}{\kappa} R_\square^*(v) \quad \forall v \in \mathcal{V}_\square^s,$$

an explicit error estimator, see (101), is derived and given by

$$\| \kappa e^s \pm \frac{1}{\kappa} e^{*s} \| \leq \left[ \int_0^T \left[ \frac{\| \Pi_C A \|_m}{\sqrt{\lambda_{NR}}} + \| \Pi_C B \|_\alpha \right]^2 dt + 2 \| \Pi_C C \|_m^2 + 2 \| \Pi_C D \|_m^2 \right]^{1/2},$$

where  $A, B, C$  and  $D$  arise from combinations of the primal and dual solutions.

#### 4. Numerical results

##### 4.1. A one-dimensional numerical example

Numerical results are obtained for an RVE of length  $l_\square$  in 1D-space (for the sake of simplicity) subjected to Dirichlet boundary conditions. The considered RVE has given  $k(x)$ ,  $c(x)$  represents the stationary homogenized thermal conductivity and heat capacity on the RVE and prescribed loading

$$\bar{u}(t) = \bar{U} \left[ 1 - \operatorname{erf} \left( \sqrt{\frac{\bar{c}}{4\bar{k}}} \frac{7l_\square}{\sqrt{t}} \right) \right], \quad \bar{g}(t) = -\frac{\bar{U}\sqrt{\bar{c}}}{\sqrt{\pi\bar{k}t}} \exp \left( -\frac{49\bar{c}l_\square^2}{4\bar{k}t} \right). \tag{120}$$

**Remark.** The data corresponds to the solution of a simplified macroscopic problem as follows: Consider the (hypothetic) situation of heat conducting through a semi-infinite body. The corresponding transient temperature distribution  $\bar{u}(x, t)$  is determined by the problem, cf. [28],

$$\begin{cases} \bar{c} \frac{\partial \bar{u}}{\partial t} - \frac{\partial}{\partial x} \bar{k} \frac{\partial \bar{u}}{\partial x} = 0, & x, t > 0, \\ \bar{u}(x, 0) = 0, \\ \bar{u}(0, t) = \bar{U}, & t > 0, \\ \bar{u}(x, t) = 0, & \text{when } x \rightarrow \infty, \end{cases} \tag{121}$$

for given homogenized quantities  $\bar{c}, \bar{k}$  and boundary value  $\bar{U}$ . Next, we define  $\bar{u}(t) \stackrel{\text{def}}{=} \bar{u}(\bar{x}, t)$  and  $\bar{g}(t) \stackrel{\text{def}}{=} \frac{d\bar{u}}{dx}(\bar{x}, t)$  for  $\bar{x} = 7l_\square$ . The analytical calculated macroscopic quantities will work as input data to the considered RVE-problem. Moreover, the coupling between the macro- and micro-scale is shown in Fig. 3.  $\square$

The corresponding dimensionless variables are defined as

$$x' \stackrel{\text{def}}{=} \frac{x}{l_\square}, \quad t' \stackrel{\text{def}}{=} \frac{\bar{k}t}{\bar{c}l_\square^2}, \quad \bar{u}' \stackrel{\text{def}}{=} \frac{\bar{u}}{\bar{U}}, \quad \bar{g}' \stackrel{\text{def}}{=} \frac{\bar{g}l_\square}{\bar{U}}, \tag{122}$$

and the results are shown in Fig. 4.

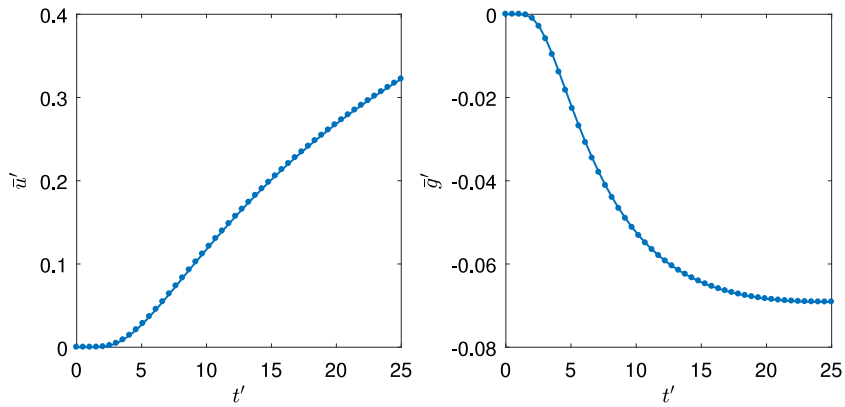


Fig. 4. Chosen loading in terms of  $\bar{u}'(t')$  and  $\bar{g}'(t')$ .

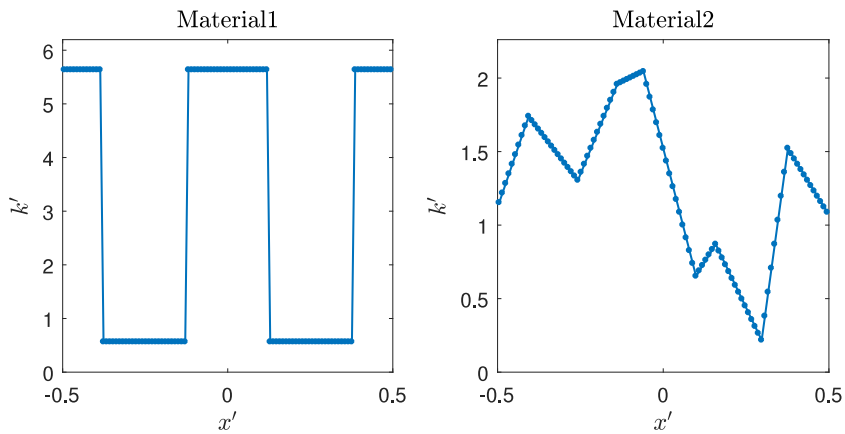


Fig. 5. Microstructure designs of relative conductivity  $k'$ . Left figure: Periodic. Right figure: Irregular.

The microstructural heterogeneity inside the RVE is defined (in this paper) in terms of a varying conductivity  $k$ , whereas the capacity  $c$  is assumed to be homogeneous. Two different microstructural arrangements are considered: Periodic variation (Material1), variation in a strongly irregular fashion (Material2). The dimensionless parameter  $k'$  and is defined as

$$k' \stackrel{\text{def}}{=} \frac{k}{\bar{k}}. \tag{123}$$

The two different microstructure designs are shown in Fig. 5.

#### 4.2. Solution of the micro-scale problem

In this Subsection we show typical results from the RVE-problem for 100 free nodal variables ( $N = 100$ ) and 50 timesteps. The results are shown in terms of dimensionless variables defined as

$$u'_\alpha \stackrel{\text{def}}{=} u_\alpha \sqrt{c l_\square}, \quad \lambda'_\alpha \stackrel{\text{def}}{=} \frac{\lambda_\alpha}{\lambda_1}, \quad \xi'_\alpha \stackrel{\text{def}}{=} \frac{\xi_\alpha}{v_0 \sqrt{c l_\square}}. \tag{124}$$

Fig. 6 shows the three first eigenmodes, whereas Fig. 7 shows the whole spectrum of eigenvalues.

Finally, Fig. 8 shows the three first mode activity coefficients. Note that  $\xi_1(t) < 0$  for Material1, while  $\xi_1(t) > 0$  for Material2. However, the contribution from the first mode is negative for both materials when  $\xi_1(t)$  is multiplied

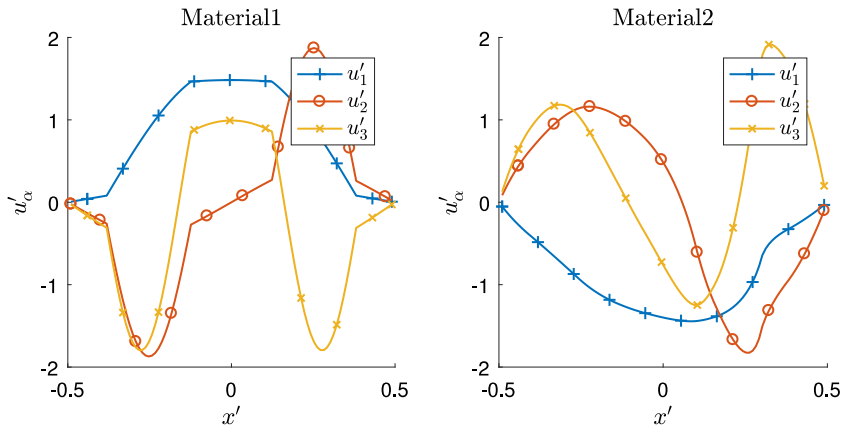


Fig. 6. Three first eigenvectors.

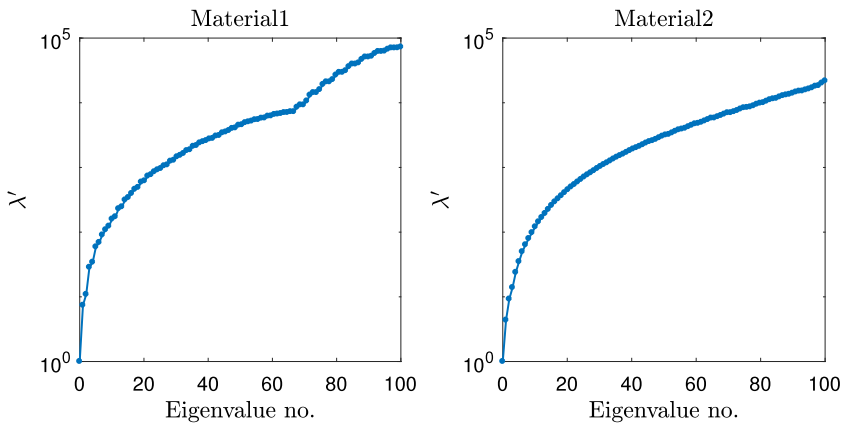


Fig. 7. Eigenvalues.

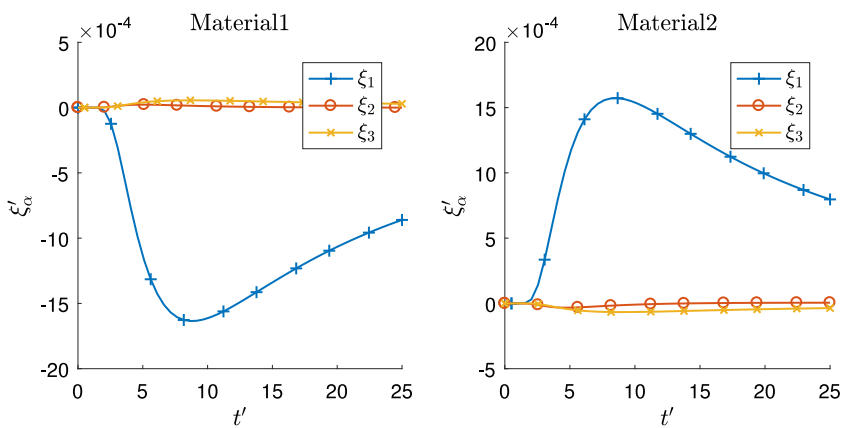


Fig. 8. Mode activity coefficients.

with the corresponding eigenmode,  $u_1(x)$ . Since the contribution from the first mode dominates, this explains why the fluctuating response is negative.

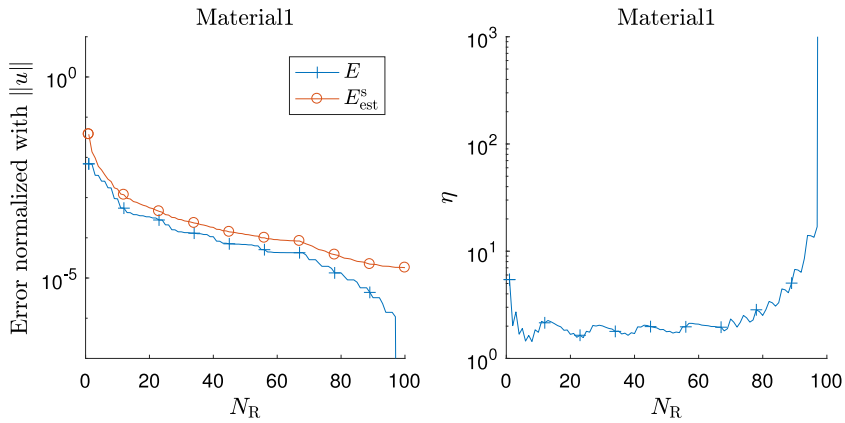


Fig. 9. Energy of error vs.  $N_R$  for  $N = 100$ , Material1: Left figure: True and estimated error. Right figure: Effectivity index.

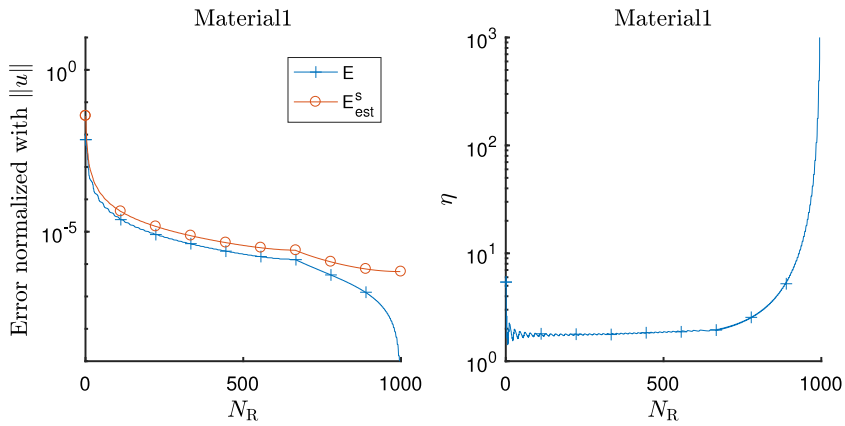


Fig. 10. Energy of error vs.  $N_R$  for  $N = 1000$ , Material1: Left figure: True and estimated error. Right figure: Effectivity index.

### 4.3. Energy norm of the error

From (112) it is recalled that the energy norm of the (true) error can be estimated by an explicit expression as follows:

$$E = \|e\| \leq E_{est}^s \quad \text{with} \quad E_{est}^s \stackrel{\text{def}}{=} \left[ \int_0^T \frac{\|II_C \dot{u}_{stat}\|_m^2}{\lambda_{N_R}} dt + 2 \|II_C u_0\|_m^2 \right]^{1/2}, \tag{125}$$

and we introduce the effectivity index,  $\eta \stackrel{\text{def}}{=} E_{est}^s / E \geq 1$ . Relative error measures are obtained upon normalizing with  $\|u\|$ , e.g. the relative true error is  $E / \|u\|$ . Results vs.  $N_R$  are shown in Figs. 9, 10 for Material1 and in Fig. 11, 12 for Material2. It is noted that  $\eta$  varies significantly with  $N_R$  for both  $N = 100$  and  $N = 1000$ . In particular,  $\eta$  increases dramatically when the higher modes are included, say for  $N_R / N > 0.7$ .

### 4.4. Error in quantity of interest

#### 4.4.1. Time-averaged homogenized stored heat

We shall first consider the time-averaged homogenized stored heat, which is given by

$$Q_{\square}(u) = \frac{1}{T} \int_0^T \bar{\Phi}(u) dt. \tag{126}$$

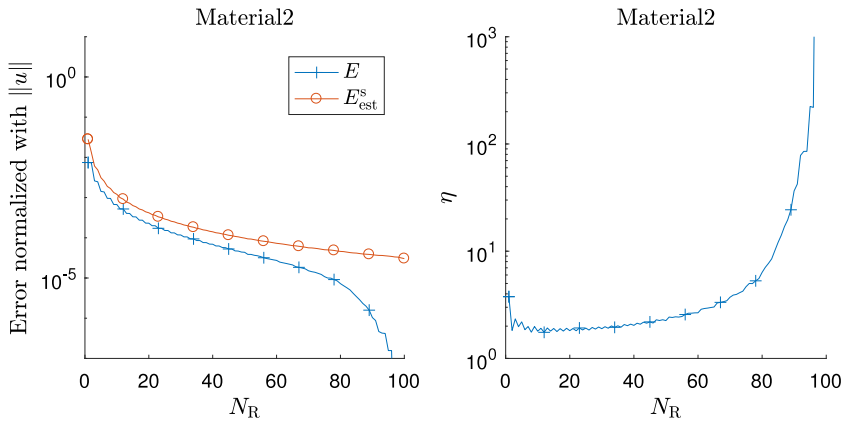


Fig. 11. Energy of error vs.  $N_R$  for  $N = 100$ , Material2: Left figure: True and estimated error. Right figure: Effectivity index.

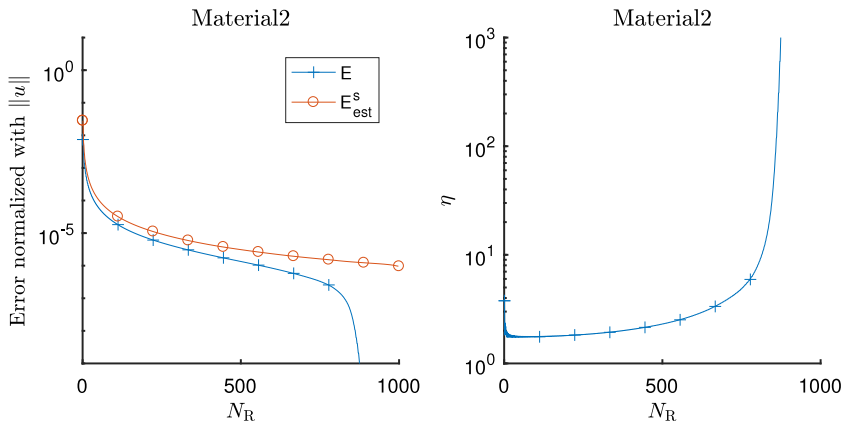


Fig. 12. Energy of error vs.  $N_R$  for  $N = 1000$ , Material2: Left figure: True and estimated error. Right figure: Effectivity index.

[For a constant heat capacity, as in the present simple model problem, this choice of  $Q_{\square}$  is equivalent to the space–time averaged temperature.] For this special case, we obtain  $X \neq 0$ , whereas  $Y = Z = 0$ .

The bounds in (118) then reduce to

$$E_{Q,\text{est}}^+ = \frac{1}{4\sqrt{\lambda_{N_R}}} \min_{\kappa \neq 0} \left[ \int_0^T \| -\kappa \Pi_C \dot{u}_{\text{stat}} + \frac{1}{\kappa} \Pi_C X \|_{\text{m}}^2 dt \right]^{1/2}, \tag{127a}$$

$$E_{Q,\text{est}}^- = -\frac{1}{4\sqrt{\lambda_{N_R}}} \min_{\kappa \neq 0} \left[ \int_0^T \| -\kappa \Pi_C \dot{u}_{\text{stat}} - \frac{1}{\kappa} \Pi_C X \|_{\text{m}}^2 dt \right]^{1/2}. \tag{127b}$$

The optimal values  $\kappa^+$  and  $\kappa^-$  are obtained explicitly as

$$\kappa = \kappa^+ = \kappa^- = \left[ \frac{\int_0^T \| \Pi_C X \|_{\text{m}}^2 dt}{\int_0^T \| \Pi_C \dot{u}_{\text{stat}} \|_{\text{m}}^2 dt} \right]^{1/4}. \tag{128}$$

Relative error measures are obtained upon normalizing with  $Q_{\square}(u)$ , e.g. the relative true error is  $E_Q/Q_{\square}(u)$ . Results vs.  $N_R$  are shown in Fig. 13 for Material1 and for Material2. Since  $N = 100$ , it is concluded that the convergence is very rapid; the error is negligible already when  $N_R/N > 0.1$ .

In order to compare with the energy norm error, it is also useful to consider an estimate of the form

$$|E_Q| \leq E_{Q,\text{est}}^{\max}, \quad E_{Q,\text{est}}^{\max} \stackrel{\text{def}}{=} \max(E_{Q,\text{est}}^+, -E_{Q,\text{est}}^-), \tag{129}$$

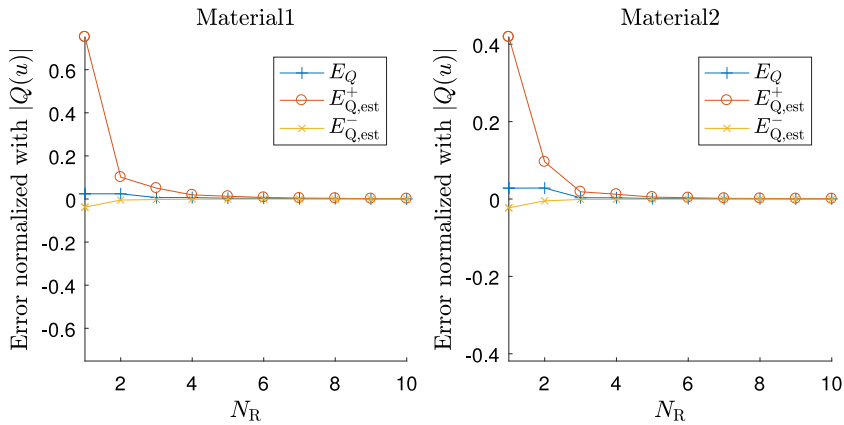


**Fig. 13.** Error in  $Q_\square$  representing time-averaged homogenized stored heat and its upper and lower bounds vs.  $N_R$  for  $N = 100$ . Left figure: Material1. Right figure: Material2.

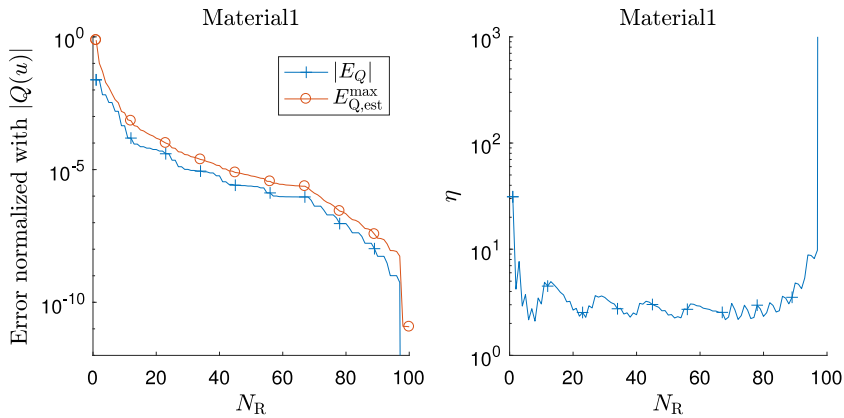


**Fig. 14.** Magnitude of error in  $Q_\square$  vs.  $N_R$  for  $N = 100$ , Material1: Left figure: True and estimated error. Right figure: Effectivity index.

and we introduce the effectivity index  $\eta \stackrel{\text{def}}{=} E_{Q,\text{est}}^{\text{max}}/|E_Q| \geq 1$ . Results vs.  $N_R$  are shown in Fig. 14 for Material1 and in Fig. 15 for Material2. Similarly to the energy norm error,  $\eta$  varies significantly with  $N_R$  (for the considered case of  $N = 100$ ) and grows dramatically when the higher modes are included. Fig. 14 confirms that the NMR-error is negligible already for  $N_R/N \approx 0.1$ . Moreover, it is seen that the effectivity index can be as low as 3 despite the very inexpensive error computation; indeed, this is a very satisfactory state of affairs since there is normally a trade-off between accuracy and low-cost in aposteriori error estimates.

4.4.2. Time-averaged homogenized heat flux

We next consider the time-averaged homogenized heat flux (single component in 1D),

$$Q_\square(u) = \frac{1}{T} \int_0^T \bar{q} dt. \tag{130}$$

For this special case, we obtain  $Y \neq 0$ , whereas  $X = Z = 0$ . The bounds in (118) then reduce to

$$E_{Q,\text{est}}^+ = \frac{1}{4} \min_{\kappa \neq 0} \left[ \int_0^T \left[ \frac{\|\kappa \Pi_C \dot{u}_{\text{stat}}\|_m}{\sqrt{\lambda_{N_R}}} + \left\| \frac{1}{\kappa} \Pi_C Y \right\|_\alpha \right]^2 dt \right]^{1/2}, \tag{131a}$$

$$E_{Q,\text{est}}^- = -\frac{1}{4} \min_{\kappa \neq 0} \left[ \int_0^T \left[ \frac{\|\kappa \Pi_C \dot{u}_{\text{stat}}\|_m}{\sqrt{\lambda_{N_R}}} + \left\| \frac{1}{\kappa} \Pi_C Y \right\|_\alpha \right]^2 dt \right]^{1/2}. \tag{131b}$$

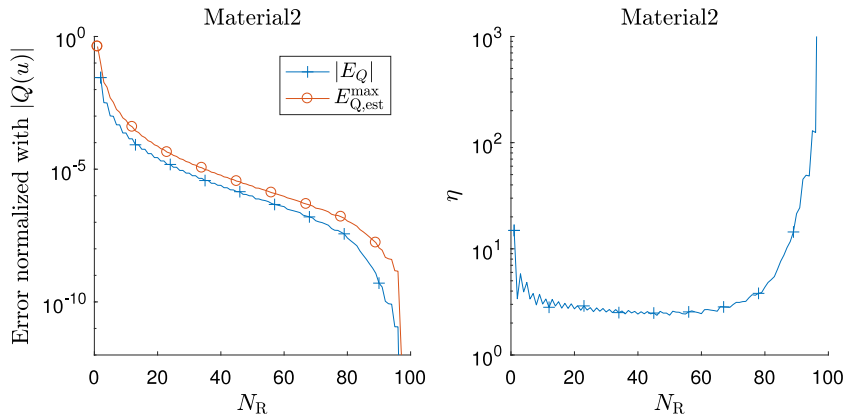


Fig. 15. Magnitude of error in  $Q_{\square}$  vs.  $N_R$  for  $N = 100$ , Material2: Left figure: True and estimated error. Right figure: Effectivity index.

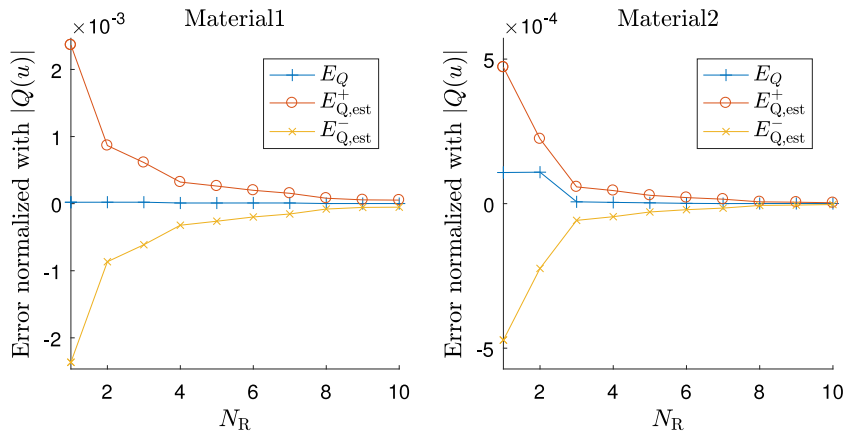


Fig. 16. Error in  $Q_{\square}$  representing time-averaged homogenized heat flux and its upper and lower bounds vs.  $N_R$  for  $N = 100$ . Left figure: Material1. Right figure: Material2.

The optimal values  $\kappa^+$  and  $\kappa^-$  are obtained explicitly as

$$\kappa = \kappa^+ = \kappa^- = \left[ \frac{\lambda_{N_R} \int_0^T \|II_C Y\|_a^2 dt}{\int_0^T \|II_C \dot{u}_{stat}\|_m^2 dt} \right]^{1/4}. \tag{132}$$

Hence,  $E_{Q,est}^+ = -E_{Q,est}^-$ .

Results vs.  $N_R$  are shown in both linear (Fig. 16) and logarithmic (Figs. 17 and 18) scale.

#### 4.4.3. Homogenized stored heat at $t = T$

Finally, we consider the homogenized stored heat at the endpoint in time,  $t = T$ ,

$$Q_{\square}(u) = \bar{\Phi}(u(\bullet, T)). \tag{133}$$

For this special case, we obtain  $Z \neq 0$ , whereas  $X = Y = 0$ . The bounds in (118) then reduce to

$$E_{Q,est}^+ = \frac{1}{4} \min_{\kappa \neq 0} \left[ \int_0^T \frac{\|\kappa II_C \dot{u}_{stat}\|_m^2}{\lambda_{N_R}} dt + 2 \left\| \frac{1}{\kappa} II_C Z \right\|_m^2 \right]^{1/2}, \tag{134a}$$

$$E_{Q,est}^- = -\frac{1}{4} \min_{\kappa \neq 0} \left[ \int_0^T \frac{\|\kappa II_C \dot{u}_{stat}\|_m^2}{\lambda_{N_R}} dt + 2 \left\| \frac{1}{\kappa} II_C Z \right\|_m^2 \right]^{1/2}. \tag{134b}$$

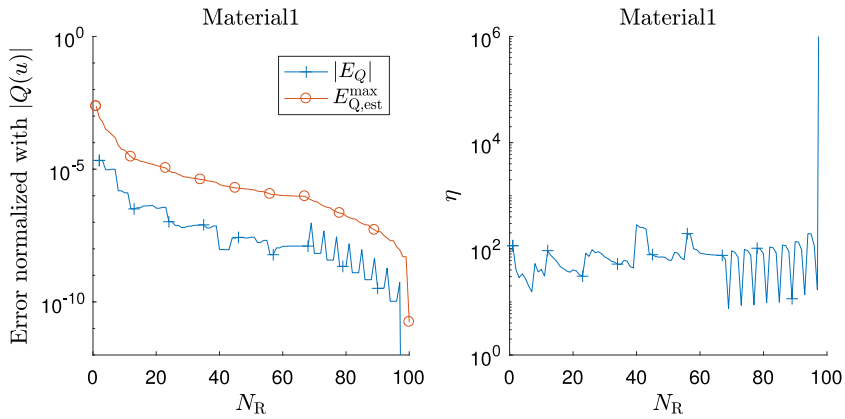


Fig. 17. Magnitude of error in  $Q_{\square}$  vs.  $N_R$  for  $N = 100$ , Material1: Left figure: True and estimated error. Right figure: Effectivity index.

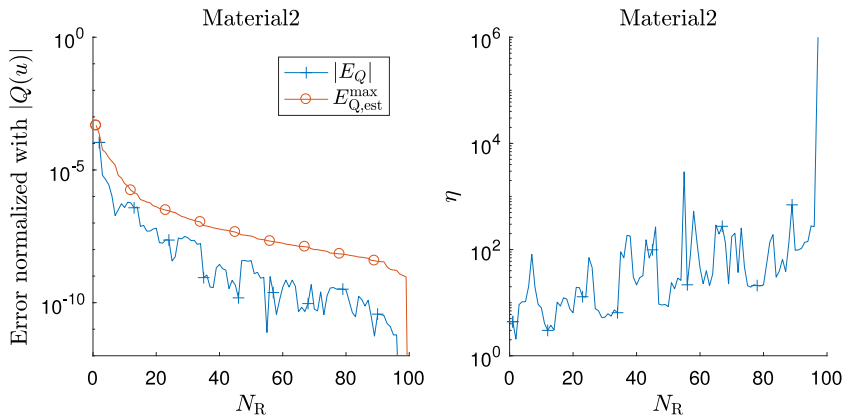


Fig. 18. Magnitude of error in  $Q_{\square}$  vs.  $N_R$  for  $N = 100$ , Material2: Left figure: True and estimated error. Right figure: Effectivity index.

The optimal values  $\kappa^+$  and  $\kappa^-$  are obtained explicitly as

$$\kappa = \kappa^+ = \kappa^- = \left[ \frac{2\lambda_{N_R} \|II_C Z\|_m^2}{\int_0^T \|II_C \dot{u}_{stat}\|_m^2 dt} \right]^{1/4}. \tag{135}$$

Hence,  $E_{Q,est}^+ = -E_{Q,est}^-$ .

Results vs.  $N_R$  are shown in both linear (Fig. 19) and logarithmic (Figs. 20 and 21) scale.

#### 4.5. Sources of NMR-errors in the error estimate

Let us recall the basic estimate in (90). Firstly, we note that the bounds are guaranteed for a given discretization (even if they are not necessarily sharp). Secondly, we may identify two main sources of errors associated with the two different steps in the “algorithm” leading to the two levels of estimated error bounds:

- *Symmetrization error:* This error is estimated by the bounds  $E_Q^+, E_Q^-$ , whereby it is noted that *all* modes are required in order to obtain the exact values of these bounds. In other words, if not all modes are used, these bounds cannot be strictly guaranteed.
- *Explicit error:* This error is represented by the difference between  $E_{Q,est}^+$  and  $E_Q^+$  and between  $E_{Q,est}^-$  and  $E_Q^-$ , respectively. It is recalled that, in order to compute the estimated bound  $E_{Q,est}^+$ , we employed only the reduced set of modes together with a further use of Cauchy–Schwarz inequality. Although the resulting bound is less sharp, it becomes very inexpensive.

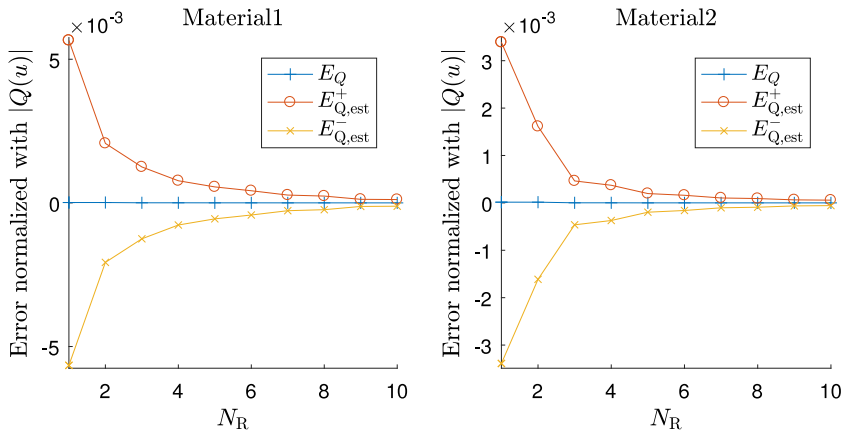


Fig. 19. Error in  $Q_{\square}$  representing homogenized stored heat at  $t = T$  and its upper and lower bounds vs.  $N_R$  for  $N = 100$ . Left figure: Material1. Right figure: Material2.

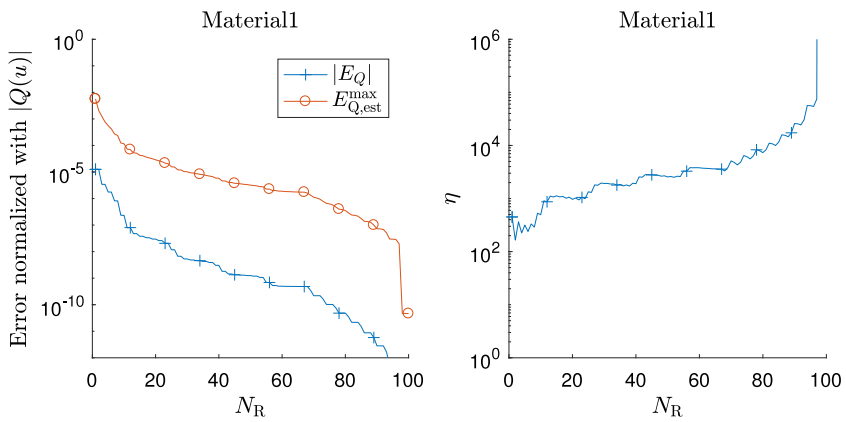


Fig. 20. Magnitude of error in  $Q_{\square}$  vs.  $N_R$  for  $N = 100$ , Material1: Left figure: True and estimated error. Right figure: Effectivity index.

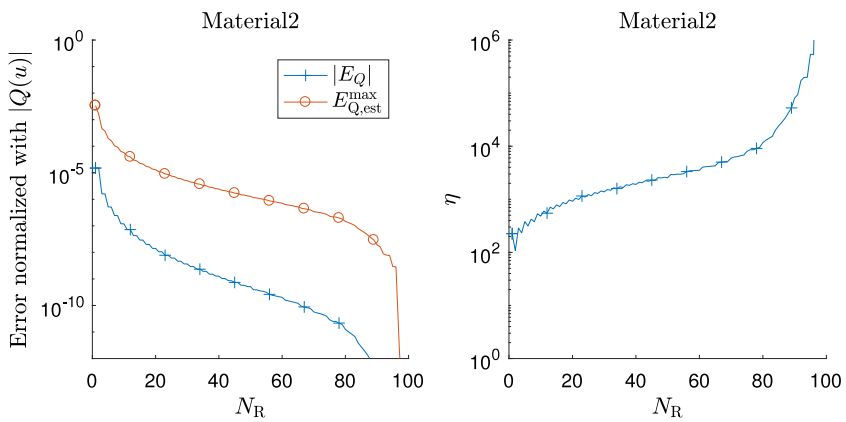
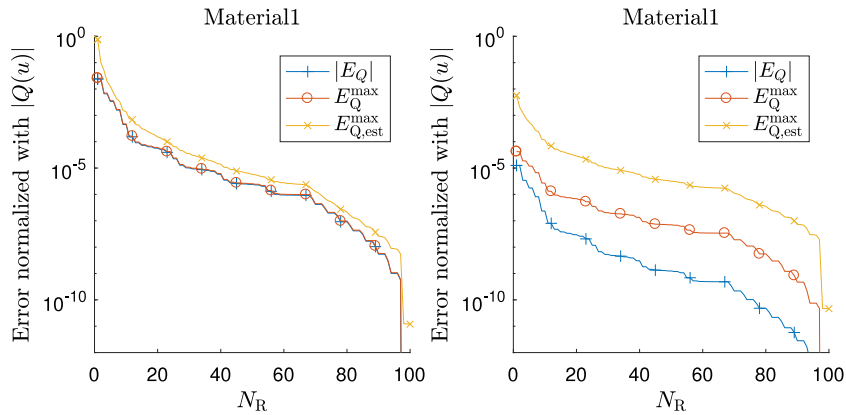


Fig. 21. Magnitude of error in  $Q_{\square}$  vs.  $N_R$  for  $N = 100$ , Material2: Left figure: True and estimated error. Right figure: Effectivity index.

In Fig. 22 we consider the estimate

$$|E_Q| \leq E_Q^{\max} \leq E_{Q,\text{est}}^{\max}, \quad E_Q^{\max} \stackrel{\text{def}}{=} \max(E_Q^+, -E_Q^-), \quad E_{Q,\text{est}}^{\max} \stackrel{\text{def}}{=} \max(E_{Q,\text{est}}^+, -E_{Q,\text{est}}^-), \quad (136)$$



**Fig. 22.** Magnitude of true and estimated error in  $Q_{\square}$  vs.  $N_R$  for  $N = 100$ .  $E_Q^{\max}$  represents symmetrization error, whereas  $E_{Q,\text{est}}^{\max}$  represents the combined effect of symmetrization and explicit error. Material1. Left figure:  $Q_{\square}$  representing time-averaged homogenized stored heat. Right figure:  $Q_{\square}$  representing homogenized stored heat at  $t = T$ .

which represents the obvious extension of (129). It is readily concluded that the symmetrization error becomes very small for the QoI representing the time/averaged stored heat (left part of the figure), whereas it becomes significant when the QoI concerns the endpoint of the time interval (right part of the figure). The converse situation is at hand for the explicit error estimate; indeed, it becomes significant for the QoI representing the time-averaged stored heat, whereas it is a smaller part for the QoI representing the endpoint of the time interval.

#### 4.6. Three-dimensional subscale resolution

For the macroscopic problem defined in Section 4.1, the modeling of the subscale is extended to three spatial dimensions. In the pertinent scale-transition, we assume a uniaxial macroscale temperature gradient. Like for the 1D-model of the subscale, the conductivity is scaled with the homogenized conductivity  $\bar{k}_{11}$  as<sup>5</sup>

$$k' \stackrel{\text{def}}{=} \frac{k}{\bar{k}_{11}}. \quad (137)$$

The microstructure is characterized by a periodic arrangement of spherical inclusions, with ten times lower conductivity (denoted Material3), cf. Fig. 23(a). Moreover, the first three modes are shown in Fig. 23(b) to (d).

Results for the energy norm error  $E$  vs.  $N_R$  are shown in Fig. 24. As for the one-dimensional RVE, the effectivity index increases with increasing  $N_R$  (see Figs. 9 to 12). Finally, the error in time-average homogenized stored heat is estimated, cf. Eq. (126), and presented in Fig. 25. Even for this particular quantity of interest, strong similarities with the results for Material1 and Material2 (see Figs. 13 to 15) can be seen.

#### 4.7. Computational efficiency

The purpose of introducing Numerical Model Reduction (NMR) is to reduce the computational cost of solving the RVE-problem. Fig. 26 shows the computational time (relative to a standard FE approach) as function of  $N_R$  for both 1D and 3D RVE-computations. For both RVE-models,  $N = 729$  and 200 timesteps are used. From the figure it is readily seen that the most time consuming operation is to solve the eigenvalue problems to obtain the (reduced) basis  $(\lambda_{\alpha}, u_{\alpha})$ . It is also concluded that performing the explicit error estimate is inexpensive (compared to solving the eigenvalue problem), and the cost does not significantly depend on  $N_R$ . In the figure we also show, for the sake of comparison, the computational effort in solving the RVE-problem using the standard time-incrementation approach arising from the Backward Euler method (standard FE). The standard FE approach is more computational demanding in 3D compared to 1D simulations (also when the same total number of nodes are used). Since the computational cost of the NMR calculations is scaled with the computational cost of the standard FE approach, the relative time for

<sup>5</sup> Note that no requirements are placed on the conductivity in other directions even though the macroscopic problem is in 1D.

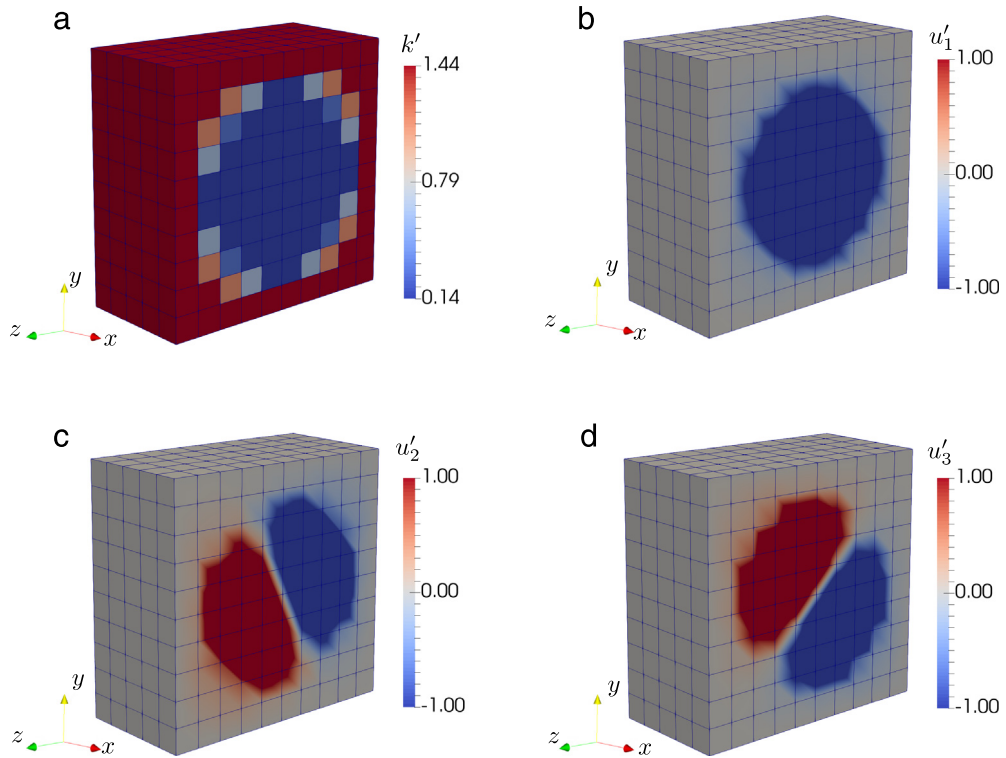


**Fig. 23.** Cut through the center of the RVE with illustrations of (a) the conductivity of the microstructure (Material3), (b) the first mode, (c) the second mode and (d) the third mode.

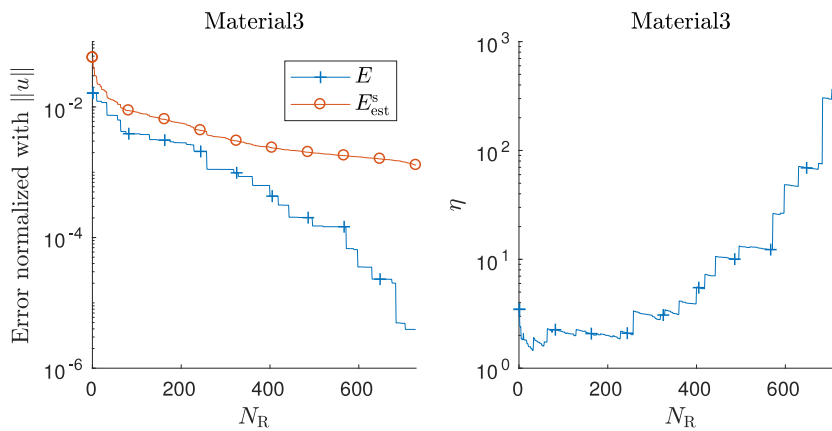


**Fig. 24.** Energy of error vs.  $N_R$  for  $N = 729$ , Material3. Left figure: True and estimated error. Right figure: Effectivity index.

solving the eigenvalue problem is smaller for the 3D simulations. The solution time of the standard FE approach is trivially independent of  $N_R$ . However, since the computational time is virtually linearly dependent on the number of time steps, it is obvious that NMR becomes more beneficial for a fine time-mesh and, hence, small time error.

### 5. Conclusions and outlook

A novel strategy for the numerical model reduction combined with error control in the context of computational homogenization of transient heat flow has been proposed and implemented successfully, albeit in one spatial

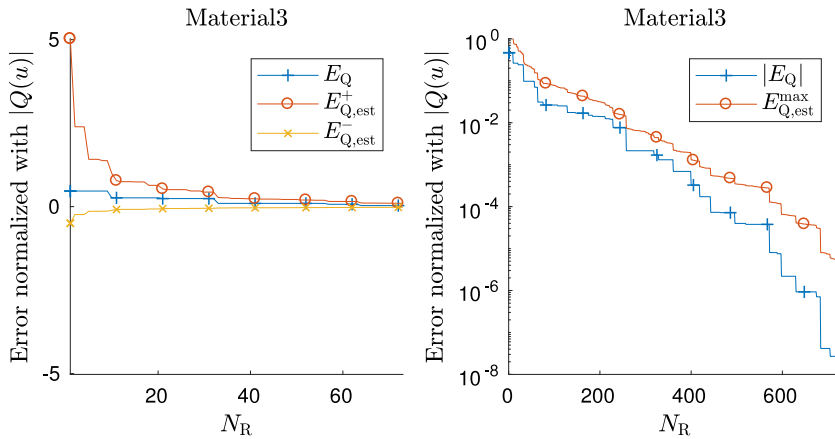


**Fig. 25.** Error in  $Q_\square$  representing time-average homogenized stored heat vs.  $N_R$  for  $N = 729$ , Material3. Left figure: Upper and lower bounds. Right figure: True and estimated error.

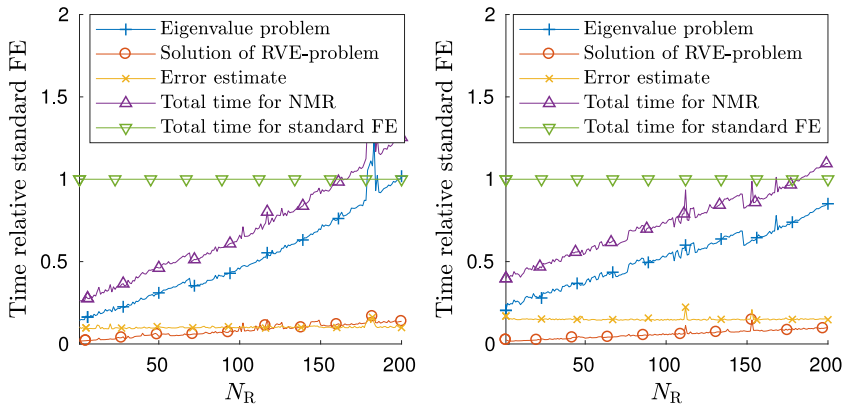


**Fig. 26.** Computational time for NMR (comprising computation of modes, solution of RVE-problem and error estimate) relative to the standard FE approach. The number of time steps is 200 and  $N = 729$ . Left figure: 1D RVE. Right figure: 3D RVE.

dimension. Due to the assumed linearity (that is, of course, a significant oversimplification for many practical problems of engineering interest), it is natural to base the NMR-strategy on classical Spectral Decomposition. The key ingredients in the error estimation are of two types: (i) use of a symmetrized space–time variational form that eliminates the time-derivative, and (ii) use of Cauchy–Schwarz inequality in such a fashion that it is possible to obtain explicit (and thereby very inexpensive) estimates that are based only on the set of reduced modes. Such an explicit estimate is established for the “symmetrized primary solution error” as well as for the “symmetrized dual solution error”. Moreover, these estimates provide guaranteed upper and lower bounds at virtually no extra cost. It is noted that only the NMR-error is accounted for, i.e. all discretization error and other solution errors are ignored. This means that the discrete solution employing all spatial modes is considered as the exact solution. Once again, it is noted that the present strategy uses only the (already computed) modes used for the NMR-approximation. The price to pay for this inexpensive estimation at the error is, obviously, a larger effectivity index; however, this drawback is considered as acceptable.

As to future extensions of the proposed strategy and the associated developments, the obvious extension is to investigate the NMR-error in the FE<sup>2</sup>-setting, which means to account for the “transfer” of error from the RVE-solution to the macroscale solution. Further, the extension of the bounds to account for the total error (including spatial as well as temporal discretization error) will be considered. In particular, this means that the (finite element) approximation of the eigenvalue problem must be considered. Since the chosen strategy relies heavily on the orthogonality properties of the chosen reduced basis (and the fact that the NMR-representation is merely a truncation of the complete=exact

solution), it does not seem feasible to apply it to nonlinear problems. However, it is desirable and natural to extend the range of application to linear coupled problems. One area is coupled consolidation in geomechanics, whereby the pertinent fields are displacement and pore pressure. In particular, the problem of wave attenuation in geological media can be represented as linear on the subscale. So far, NMR for this problem was developed by Jänicke et al. [10] using a POD-basis but without error estimation. The ultimate goal is to devise an adaptive method for the choice of a reduced basis.

## Acknowledgments

This research was supported by the Swedish Research Council (VR), grant no. 2015-05422.

## Appendix. Computation of symmetrization error

### A.1. Generic error equation

In order to compute the bounds  $E_Q^+$  and  $E_Q^-$  exactly, we need to find the exact solutions  $e^s$  and  $e^{*s}$ . To this end, we (re)consider the generic equations (97) from which  $\chi$  can be computed. Firstly, consider (97a) and seek  $\chi \in \mathbb{U}_\square^0$  for  $t \in (0, T)$  s.t.

$$\mathbf{a}_\square(\chi, \delta u) = \mathbf{m}_\square(\Pi_C A, \delta u) + \mathbf{a}_\square(\Pi_C B, \delta u) \quad \forall \delta u \in \mathbb{U}_\square^0, \quad t \in (0, T). \quad (\text{A.1})$$

We recall that  $\chi$  has the representation

$$\chi(x, t) = \Pi_C \chi(x, t) = \sum_{\alpha=N_R+1}^N u_\alpha(x) \varphi_\alpha(t), \quad (\text{A.2})$$

where the coefficients  $\varphi_\alpha(t)$  will have to be determined. Setting  $\delta u = u_\beta$  for  $\beta = N_R + 1, N_R + 2, \dots, N$ , we obtain the following relation from (A.1):

$$\begin{aligned} \sum_{\beta=N_R+1}^N \mathbf{a}_\square(u_\alpha, u_\beta) \varphi_\beta &= \mathbf{m}_\square(\Pi_C A, u_\alpha) + \mathbf{a}_\square(\Pi_C B, u_\alpha) \stackrel{\text{def}}{=} f_\alpha, \\ \alpha &= N_R + 1, N_R + 2, \dots, N, \quad t \in (0, T). \end{aligned} \quad (\text{A.3})$$

Due to the orthogonality, (A.3) trivially gives the solution

$$\varphi_\alpha(t) = \frac{f_\alpha(t)}{\lambda_\alpha}, \quad \alpha = N_R + 1, N_R + 2, \dots, N, \quad t \in (0, T). \quad (\text{A.4})$$

As to the values  $\varphi_\alpha(0)$  and  $\varphi_\alpha(T)$ , we consider (97b) and (97c) to obtain the solutions

$$\varphi_\alpha(0) = \mathbf{m}_\square(2\Pi_C C, u_\alpha), \quad \varphi_\alpha(T) = \mathbf{m}_\square(2\Pi_C D, u_\alpha), \quad \alpha = N_R + 1, N_R + 2, \dots, N. \quad (\text{A.5})$$

### A.2. Symmetrized primary problem

Setting  $\chi = e^s$ , we obtain from (A.4) and (A.5) the corresponding solutions

$$\varphi_\alpha^s(t) = \frac{\mathbf{m}_\square(-\Pi_C \dot{u}_{\text{stat}}, u_\alpha)}{\lambda_\alpha}, \quad \alpha = N_R + 1, N_R + 2, \dots, N, \quad t \in (0, T), \quad (\text{A.6})$$

$$\varphi_\alpha^s(0) = \mathbf{m}_\square(2\Pi_C u_0, u_\alpha), \quad \varphi_\alpha^s(T) = 0, \quad \alpha = N_R + 1, N_R + 2, \dots, N. \quad (\text{A.7})$$

### A.3. Symmetrized dual problem

Setting  $\chi = e^{*s}$ , we obtain from (A.4) and (A.5) the corresponding solutions

$$\varphi_\alpha^{*s}(t) = \frac{\mathbf{m}_\square(\Pi_C X, u_\alpha) + \mathbf{a}_\square(\Pi_C Y, u_\alpha)}{\lambda_\alpha}, \quad \alpha = N_R + 1, N_R + 2, \dots, N, \quad t \in (0, T), \quad (\text{A.8})$$

$$\varphi_\alpha^{*s}(0) = 0, \quad \varphi_\alpha^{*s}(T) = \mathbf{m}_\square(2\Pi_C Z, u_\alpha), \quad \alpha = N_R + 1, N_R + 2, \dots, N. \quad (\text{A.9})$$

## References

- [1] C. Oskay, J. Fish, Eigendeformation-based reduced order homogenization for failure analysis of heterogeneous materials, *Comput. Methods Appl. Mech. Engrg.* 196 (7) (2007) 1216–1243.
- [2] J. Fish, Z. Yuan, Multiscale enrichment based on partition of unity for nonperiodic fields and nonlinear problems, *Comput. Mech.* 40 (2) (2007) 249–259.
- [3] G.J. Dvorak, Y. Benveniste, On transformation strains and uniform fields in multiphase elastic media, *Proc. R. Soc. Lond. Ser. A Math. Phys. Eng. Sci.* 437 (1992) 291–310.
- [4] J.-C. Michel, P. Suquet, Nonuniform transformation field analysis, *Int. J. Solids Struct.* 40 (25) (2003) 6937–6955.
- [5] J.-C. Michel, P. Suquet, Computational analysis of nonlinear composite structures using the nonuniform transformation field analysis, *Comput. Methods Appl. Mech. Engrg.* 193 (48) (2004) 5477–5502.
- [6] F. Fritzen, T. Böhlke, Three-dimensional finite element implementation of the nonuniform transformation field analysis, *Internat. J. Numer. Methods Engrg.* 84 (7) (2010) 803–829.
- [7] F. Fritzen, M. Hodapp, M. Leuschner, GPU accelerated computational homogenization based on a variational approach in a reduced basis framework, *Comput. Methods Appl. Mech. Engrg.* 278 (2014) 186–217.
- [8] J. Hernández, J. Oliver, A.E. Huespe, M. Caicedo, J. Cante, High-performance model reduction techniques in computational multiscale homogenization, *Comput. Methods Appl. Mech. Engrg.* 276 (2014) 149–189.
- [9] N.C. Nguyen, A multiscale reduced-basis method for parametrized elliptic partial differential equations with multiple scales, *J. Comput. Phys.* 227 (23) (2008) 9807–9822.
- [10] R. Jänicke, F. Larsson, K. Runesson, H. Steeb, Numerical identification of a viscoelastic substitute model for heterogeneous poroelastic media by a reduced order homogenization approach, *Comput. Methods Appl. Mech. Engrg.* 298 (2016) 108–120.
- [11] Y. Efendiev, J. Galvis, F. Thomines, A systematic coarse-scale model reduction technique for parameter-dependent flows in highly heterogeneous media and its applications, *Multiscale Model. Simul.* 10 (4) (2012) 1317–1343.
- [12] P. Ladevèze, L. Chamoin, On the verification of model reduction methods based on the proper generalized decomposition, *Comput. Methods Appl. Mech. Engrg.* 200 (23) (2011) 2032–2047.
- [13] M. Cremonesi, D. Néron, P.-A. Guidault, P. Ladevèze, A PGD-based homogenization technique for the resolution of nonlinear multiscale problems, *Comput. Methods Appl. Mech. Engrg.* 267 (2013) 275–292.
- [14] A. Abdulle, Y. Bai, Adaptive reduced basis finite element heterogeneous multiscale method, *Comput. Methods Appl. Mech. Engrg.* 257 (2013) 203–220.
- [15] S. Boyaval, Reduced-basis approach for homogenization beyond the periodic setting, *Multiscale Model. Simul.* 7 (1) (2008) 466–494.
- [16] D.-A. Paladim, J. Moitinho de Almeida, S. Bordas, P. Kerfriden, Guaranteed error bounds in homogenisation: An optimum stochastic approach to preserve the numerical separation of scales, *Internat. J. Numer. Methods Engrg.* 110 (2) (2017) 103–132.
- [17] M. Ohlberger, F. Schindler, Error control for the localized reduced basis multiscale method with adaptive on-line enrichment, *SIAM J. Sci. Comput.* 37 (6) (2015) A2865–A2895.
- [18] P. Kerfriden, J.-J. Ródenas, S.-A. Bordas, Certification of projection-based reduced order modelling in computational homogenisation by the constitutive relation error, *Internat. J. Numer. Methods Engrg.* 97 (6) (2014) 395–422.
- [19] C. Jhurani, L. Demkowicz, Multiscale modeling using goal-oriented adaptivity and numerical homogenization. Part I: Mathematical formulation and numerical results, *Comput. Methods Appl. Mech. Engrg.* 213 (2012) 399–417.
- [20] F. Larsson, K. Runesson, RVE computations with error control and adaptivity: The power of duality, *Comput. Mech.* 39 (5) (2007) 647–661.
- [21] N. Parés, P. Díez, A. Huerta, Exact bounds for linear outputs of the advection-diffusion-reaction equation using flux-free error estimates, *SIAM J. Sci. Comput.* 31 (4) (2009) 3064–3089.
- [22] N. Parés, P. Díez, A. Huerta, Bounds of functional outputs for parabolic problems. Part I: Exact bounds of the discontinuous Galerkin time discretization, *Comput. Methods Appl. Mech. Engrg.* 197 (19) (2008) 1641–1660.
- [23] N. Parés, P. Díez, A. Huerta, Bounds of functional outputs for parabolic problems. Part II: Bounds of the exact solution, *Comput. Methods Appl. Mech. Engrg.* 197 (19) (2008) 1661–1679.
- [24] H. Jakobsson, F. Bengzon, M.G. Larson, Adaptive component mode synthesis in linear elasticity, *Internat. J. Numer. Methods Engrg.* 86 (7) (2011) 829–844.
- [25] F. Larsson, K. Runesson, F. Su, Variationally consistent computational homogenization of transient heat flow, *Internat. J. Numer. Methods Engrg.* 81 (13) (2010) 1659–1686.
- [26] M.C. Bampton, R.R. Craig Jr, Coupling of substructures for dynamic analyses, *AIAA J.* 6 (7) (1968) 1313–1319.
- [27] T. Hawkins, Cauchy and the spectral theory of matrices, *Hist. Math.* 2 (1) (1975) 1–29.
- [28] J. Crank, *The Mathematics of Diffusion*, second ed., Clarendon Press, 1975.